Aus dem
Comprehensive Pneumology Center (CPC)
Institut für Experimentelle Pneumologie der Ludwig-Maximilians-Universität München
Kommissarische Leitung: Dr. Antje Brand

# Validation of CCR2-targeted Mesoporous Silica Nanoparticles for Lung Cancer Therapy

Dissertation
zum Erwerb des Doktorgrades der Medizin
an der Medizinischen Fakultät der
Ludwig-Maximilians-Universität zu München

vorgelegt von

Charlotte Meyer-Schwickerath
aus Düsseldorf

2019

Mit Genehmigung der Medizinischen Fakultät

der Universität München

Berichterstatterin: Prof. Dr. Silke Meiners

Mitberichterstatter: PD Dr. Amanda Tufmann

Prof. Dr. Lars Lindner

Dekan: Prof. Dr. med. dent. Reinhard Hickel

Tag der mündlichen Prüfung: 07.11.2019

# Table of contents

# Zusammenfassung

Trotz diverser Fortschritte in der Behandlung von Lungenkrebs, führen maligne Lungentumore weiterhin die Liste der Tumor-assoziierten Todesfälle an. Mit einer 5-Jahres Überlebensrate von 15,9% gehört Lungenkrebs immer noch zu den Krankheiten mit der höchsten Mortalität weltweit. Da eine frühzeitige Erkennung von Lungentumoren weiterhin schwierig ist, ist auch eine frühzeitige Behandlung vielfach nicht möglich. Ein Schwerpunkt in der Entwicklung von neuen Therapien für Tumorerkrankungen in den letzten Jahren liegt daher zum Einen auf der Behandlung des tumorumgebenden Milieus, das aus verschiedenen Zellarten besteht. Gerade Tumorassoziierte Makrophagen spielen darin eine wichtige Rolle und sind in den letzten Jahren in den Fokus möglicher Therapien gerückt. Zum Anderen wurden vermehrt Studien zu zielgerichteten Therapien durchgeführt. Die Idee ist, spezifisch nur Tumorzellen oder Zellen des tumorumgebenden Milieus zu eliminieren und so gesundes Gewebe zu schonen und Nebenwirkungen zu reduzieren. Eine Möglichkeit solch einer zielgerichteten Therapie ist ein Nanopartikel-basierter Therapieansatz. Die Nanometer großen Partikel bestehen aus unterschiedlichsten organischen und anorganischen Materialien und können z.B. so entwickelt werden, dass eingeschlossene Chemotherapeutika nur auf bestimmte Stimuli hin entweichen können. Außerdem können Liganden angebracht werden, die an bestimmte nur auf den Zielzellen exprimierte Rezeptoren binden, und so eine rezeptorspezifische Aufnahme der Nanotherapeutika in den Zielzellen sicherstellen.

Unsere Kooperationspartner haben zu diesem Zweck mesoporöse Siliziumnanopartikel (MSNs) entwickelt, aus denen die eingeschlossenen Therapeutika nur im sauren Milieu entweichen können. Zudem wurden Liganden befestigt, die spezifisch mit Rezeptoren auf Lungenkarzinomzellen reagieren und so eine Rezeptor-gesteuerte Aufnahme der MSNs in die Zielzellen erwirken können. Das Ziel der vorliegenden Arbeit war die Evaluation von zielgerichteten MSNs, die an den CCR2 Rezeptor binden, der vor allem auf Lungenkarzinomzellen und Tumorassoziierten Makrophagen von Lungenkarzinompatienten über-exprimiert ist.

Zur Beurteilung der genannten Partikel wurde ein Studiendesign mit *in vitro*, *ex vivo* und *in vivo* Experimenten entwickelt. Zunächst konnten wir feststellen, dass

der CCR2 Rezeptor sowohl in humanen Lungenkarzinomproben, als auch in Tumoren des K-ras$^{tm3Tyj}$ Maus Modells, ein etabliertes Tiermodell für Lungenkarzinome, über-exprimiert ist. Zudem nahmen CCR2 exprimierende MHS Zellen die zielgerichteten Nanopartikel deutlich stärker auf, als ungerichtete Kontrollpartikel. Die Ergebnisse eines *ex vivo* Ansatzes, bei dem vitale Lungensektionen aus K-ras$^{tm3Tyj}$ Maus Lungen mit MSNs behandelt wurden, konnten auf Grund von experimentellen Problemen nicht verwertet werden. Der daraufhin entwickelte *in vivo* Ansatz zeigte jedoch gegensätzliche Befunde zum vorherigen *in vitro* Ansatz, da Tumore und tumorfreie Regionen der intratracheal behandelten K-ras$^{tm3Tyj}$ Mäuse eine ähnliche Aufnahme der zielgerichteten MSNs und Kontrollpartikeln zeigten. Im Gegenteil, Kontrollpartikel und zielgerichtete MSNs wurden in gleichem Maße von Alveolarmakrophagen aufgenommen, obwohl diese eine hohe Expression von CCR2 zeigten .

Zusammenfassend lässt sich sagen, dass unsere Daten bereits vorhandene Daten zur Überexpression und der wichtigen Rolle des CCR2 Rezeptors in der Entwicklung des Lungenkarzinoms bestätigen. Auch die Möglichkeit einer zielgerichteten Therapie gegen diesen Rezeptor wurde noch einmal bekräftigt. Allerdings konnten wir einen Funktionsverlust des zielgerichteten Therapieversuchs *in vivo* beobachten, obwohl dieser Ansatz *in vitro* gute Ergebnisse erzielte. Dies bestätigt zum Einen die wichtige Rolle von Alveolarmakrophagen in der Beseitigung von Nanopartikeln, die lokal der Lunge zugeführt werden. Zum Anderen zeigt es auf, dass detaillierte *in vivo* Experimente zur Beurteilung der therapeutischen Effektivität funktionalisierter Nanopartikeln notwendig sind.

# Summary

Lung cancer has one of the highest mortality rates worldwide and even though advancements in treatment schemes have been made over the last years, lung cancer stays on top of the list for causes of cancer related deaths with a 5-year survival rate of 15,9%. In addition, early diagnosis and thus early treatment for lung cancer has not been achieved yet. In the past years treating the cancer microenvironment and especially tumor-associated macrophages has been a major field of discussion. In addition, an emphasis on new targeted therapy strategies for cancer treatment has been made. As the idea is to target only tumor cells, healthy tissue should be spared and hence side effects of the therapy should be reduced. One approach to actively target tumor cells and tumor-associated macrophages is with the help of nanoparticles. These nanometer size particles can consist of different materials and can, for example, encapsulate chemotherapeutics to release them at a specific stimulus. In addition, ligands can be attached to actively target cells expressing a fitting receptor.

For this purpose, our collaborators designed mesoporous silica nanoparticles (MSNs) in a way that they release their cargo only in an acidic environment. In addition, for active targeting these MSNs can be functionalized by adding a targeting ligand binding to receptors highly expressed in lung cancer. Hence the aim of this thesis was to validate CCR2-targeted mesoporous silica nanoparticles for a targeted therapy approach to lung cancer, as the CCR2 receptor is commonly overexpressed on cancer cells and tumor-associated macrophages in lung cancer patients.

For the evaluation of the CCR2-targeted MSNs an *in vitro*, *ex vivo* and *in vivo* experimental setup was designed. Firstly, we could confirm the expression of CCR2 in human lung cancer samples and tumors of K-ras$^{tm3Tyj}$ mice, a well-established lung cancer animal model. Secondly, we could show an increased uptake of CCR2-targeted MSNs in CCR2 expressing MHS cells in comparison to the control particles. Thirdly, *ex vivo* lung slices of K-ras$^{tm3Tyj}$ mice were treated with MSNs and uptake differences in tumor and tumor free regions was assessed. However, experimental difficulties led to the discard of these results. Following, an *in vivo* approach in which K-ras$^{tm3Tyj}$ mice were treated with the named particles by intratracheal administration was conducted. Interestingly, the positive *in*

*vitro* results could not be observed, as no difference in uptake of CCR2-targeted MSNs in tumor and tumor free regions could be noticed and alveolar macrophages incorporated CCR2-targeted and control particles to a similar extent yet expressing a high amount of CCR2 receptors.

Taken together, our data confirms recent studies stating the importance of the CCR2 receptor in lung cancer development and the possibility of using this receptor as a target for specific therapy approaches. However, as we show a loss of targeting abilities of functionalized MSNs *in vivo,* out data stress the importance of alveolar macrophages in the clearing process of nanoparticles when administered locally to the lung. In addition, the lost targeting capacities of the MSNs underline the need for careful *in vivo* studies of functionalized targeted nanoparticles.

# 1 Introduction

## 1.1 Lung cancer

### 1.1.1 Lung cancer epidemiology and symptoms

Lung cancer has one of the highest incidence rates of cancers worldwide and is the leading cause of cancer-associated deaths in the United States (Ferlay J, 2012; Siegel, Miller, & Jemal, 2017) with a 5-year survival rate of 15.9% (Chen, Fillmore, Hammerman, Kim, & Wong, 2014; Herold, 2017, pp. 400-405). In Germany, it is the leading cause of cancer associated deaths of males (25%), and ranked second for females (15%). In 2013, 29.708 males und 15.140 females died due to lung cancer in Germany ("Leitlinienprogramm Onkologie, 2017,")

The leading risk factor associated with lung cancer is smoking, which is responsible for 85% of all lung carcinomas. The cancer risk depends on the amount of smoked cigarettes, which is estimated in pack-years (=number of daily consumed cigarette packages times number of years the patient is smoking) (Herold, 2017, pp. 400-405). 30 pack-years increase the cancer risk tenfold. Further, Secondhand smoke (SHS) can also significantly increase the risk of the disease by factor 1.3 - 2. In addition, exposure to carcinogenic factors such as asbestos, arsenic, ionizing radiation and radon at work or at home increase the risk to develop lung cancer (Herold, 2017, pp. 400-405). Moreover, patients having an underlying lung disease such as COPD, chronic bronchitis, emphysema or pulmonary fibrosis are more likely to develop lung cancer than healthy individuals (Collins, Haines, Perkel, & Enck, 2007; Avrum Spira, Halmos, & Powell, 2015; A. Spira, Halmos, & Powell, 2016).

### 1.1.2 Lung cancer diagnosis

Lung cancer does not cause specific symptoms, leading to a problem in early diagnosis. Most of the patients present with non-specific manifestations, such as weight loss, fatigue, cough, dyspnea, hemoptysis and chest discomfort (Collins et al., 2007; Herold, 2017, pp. 400-405). However, lung cancer can be accompanied by systemic symptoms due to paraneoplastic syndromes, as approximately 10% of lung cancers produce bioactive substances (Collins et al., 2007; Herold,

2017). In addition, another presentation of lung cancer is the Pancost Syndrom, defined by a tumor developing in the lung apex and eroding the thoracic wall, thus leading to a Horner Syndrome (Miosis, Ptosis and Enopthalmus) as well as to swelling of the arm and neuralgic pain (Herold, 2017).

Lung tumors can first be seen with radiological imaging, such as thoracic x-ray, computer tomography (CT) or high resolution computer tomography (HRCT). Figure 1-1 displays an area with higher density in the right upper lobe of a lung on a X-Ray (a) and CT (c) scan, showing a typical result of a lung tumor. In addition, endobronchial ultrasonography can detect lung lesion (Collins et al., 2007; Herold, 2017; Avrum Spira et al., 2015). However, for specific diagnosis biopsies are needed, which can be taken via bronchoscopy while identifying lesions with autofluorescence (A. Spira et al., 2016). Other options include endoscopic ultrasonography-guided needle aspiration or video assisted thoracoscopy (Herold, 2017; Avrum Spira et al., 2015). For assessing metastasis of lung cancer, sonography, MRI, CT or PET-CT scans can be an option (Collins et al., 2007; Herold, 2017).

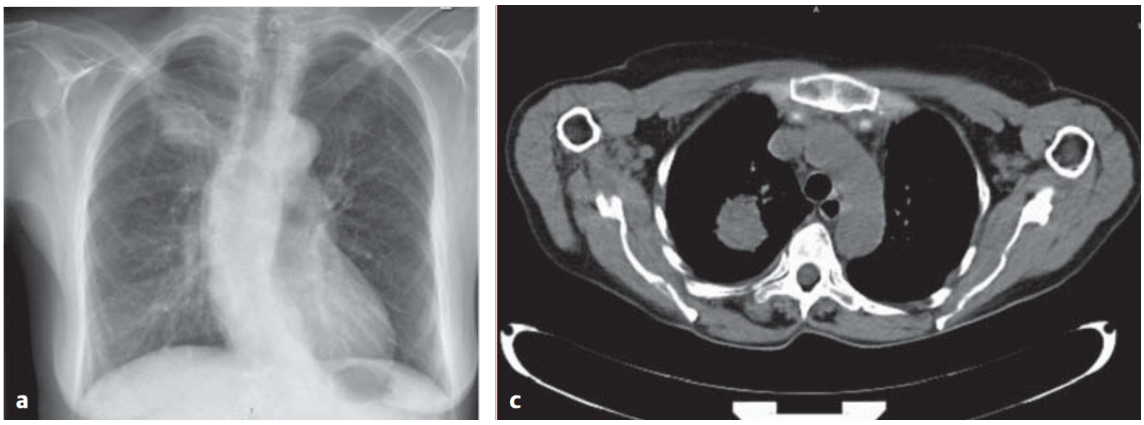


**Figure 1-1 Lung tumor in X-Ray and CT scans**

Lung tumors (area with the higher density) in the right upper lobe seen on an X-ray (a) and CT scan (c). (Figure adopted and modified from Arasteh, 2013).

As described above, early stage lung cancer causes nearly no symptoms, thus lung cancer screening has been a focus in lung cancer research in recent years. Nonetheless, there is an open debate whether screening for lung cancer with the current diagnostic modalities in the healthy population is beneficial, as only one

trial in the United States with a subject group of 55 to 77 years old smokers highly at risk for lung cancer and screening with low-dose CT showed a survival benefit in the screened group (Aberle DR, 2011). Other European studies with lower risk-populations revealed no difference in lung cancer mortality between the screening and non-screening group (Herold, 2017; A. Spira et al., 2016). However, these conclusions may be re-evaluated when better risk scores, diagnostic pathways and agents such as diagnostic biomarkers are developed (Osmani, Askin, Gabrielson, & Li, 2017; A. Spira et al., 2016).

### 1.1.3 Lung cancer classification

Histologically lung cancer can be classified into small cell lung cancer (SCLC), defined by small cells with a small amount of cytoplasm as seen in Figure 1-2, and non-small cell lung cancer (NSCLC) with the latter being the most common form (85%) (Chen et al., 2014). Non-small cell lung cancer can then be subdivided into Squamous cell carcinoma (Figure 1-2), Adenocarcinoma (Figure 1-2), Large cell carcinoma, Adenosquamos carcinoma, Sarcomatoid carcinoma, Carcinoid tumor and tumors of bronchial glands (Travis William D., 2015).

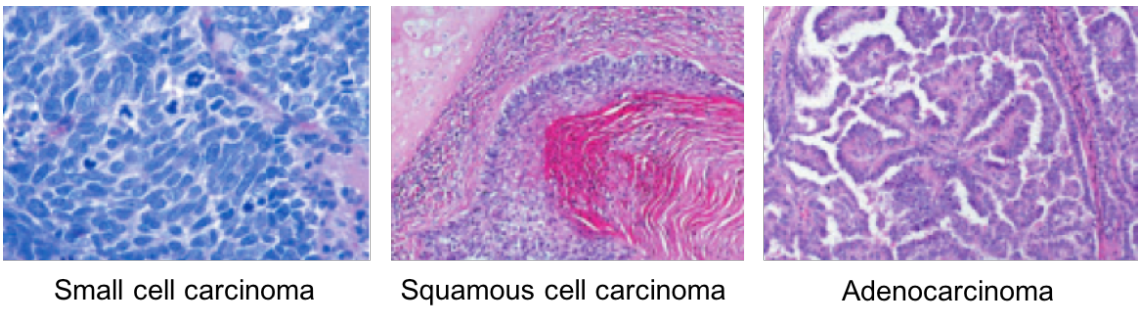


**Figure 1-2 Histological classification of lung tumors**

Selection of histological features of Small cell lung cancer, Squamous cell carcinoma and Adenocarcinoma of the lung. (Figure adopted and modified from Travis William D., 2015).

In addition, lung cancer, as all malignant tumors, can be classified by the TNM Classification (T-Tumor size and spread, N – number of tumor infected lymph nodes, M – Presence and number of metastatic lesions), which is also used for

grouping different lung tumors into a disease stage as presented in Figure 1-3 (Travis William D., 2015).

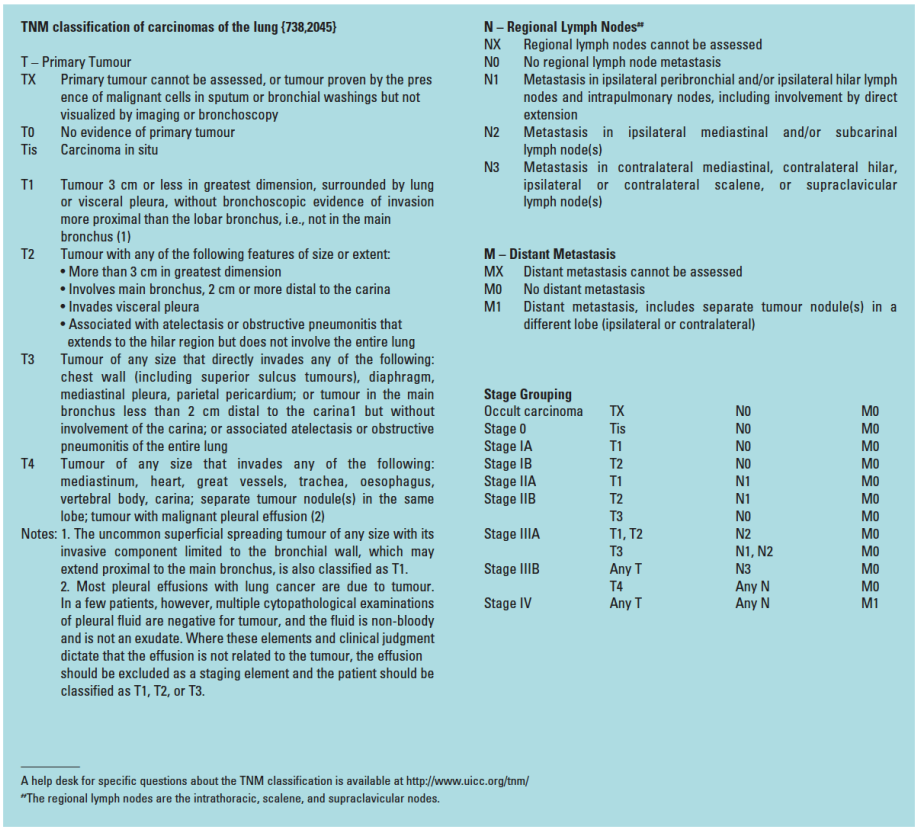

**TNM classification of carcinomas of the lung {738,2045}**

T – Primary Tumour

TX Primary tumour cannot be assessed, or tumour proven by the pres ence of malignant cells in sputum or bronchial washings but not visualized by imaging or bronchoscopy

T0 No evidence of primary tumour

Tis Carcinoma in situ

T1 Tumour 3 cm or less in greatest dimension, surrounded by lung or visceral pleura, without bronchoscopic evidence of invasion more proximal than the lobar bronchus, i.e., not in the main bronchus (1)

T2 Tumour with any of the following features of size or extent:
- More than 3 cm in greatest dimension
- Involves main bronchus, 2 cm or more distal to the carina
- Invades visceral pleura
- Associated with atelectasis or obstructive pneumonitis that extends to the hilar region but does not involve the entire lung

T3 Tumour of any size that directly invades any of the following: chest wall (including superior sulcus tumours), diaphragm, mediastinal pleura, parietal pericardium; or tumour in the main bronchus less than 2 cm distal to the carina1 but without involvement of the carina; or associated atelectasis or obstructive pneumonitis of the entire lung

T4 Tumour of any size that invades any of the following: mediastinum, heart, great vessels, trachea, oesophagus, vertebral body, carina; separate tumour nodule(s) in the same lobe; tumour with malignant pleural effusion (2)

Notes: 1. The uncommon superficial spreading tumour of any size with its invasive component limited to the bronchial wall, which may extend proximal to the main bronchus, is also classified as T1.

2. Most pleural effusions with lung cancer are due to tumour. In a few patients, however, multiple cytopathological examinations of pleural fluid are negative for tumour, and the fluid is non-bloody and is not an exudate. Where these elements and clinical judgment dictate that the effusion is not related to the tumour, the effusion should be excluded as a staging element and the patient should be classified as T1, T2, or T3.

**N – Regional Lymph Nodes[#]**

NX Regional lymph nodes cannot be assessed

N0 No regional lymph node metastasis

N1 Metastasis in ipsilateral peribronchial and/or ipsilateral hilar lymph nodes and intrapulmonary nodes, including involvement by direct extension

N2 Metastasis in ipsilateral mediastinal and/or subcarinal lymph node(s)

N3 Metastasis in contralateral mediastinal, contralateral hilar, ipsilateral or contralateral scalene, or supraclavicular lymph node(s)

**M – Distant Metastasis**

MX Distant metastasis cannot be assessed

M0 No distant metastasis

M1 Distant metastasis, includes separate tumour nodule(s) in a different lobe (ipsilateral or contralateral)

**Stage Grouping**

| | | | |
|---|---|---|---|
| Occult carcinoma | TX | N0 | M0 |
| Stage 0 | Tis | N0 | M0 |
| Stage IA | T1 | N0 | M0 |
| Stage IB | T2 | N0 | M0 |
| Stage IIA | T1 | N1 | M0 |
| Stage IIB | T2 | N1 | M0 |
| | T3 | N0 | M0 |
| Stage IIIA | T1, T2 | N2 | M0 |
| | T3 | N1, N2 | M0 |
| Stage IIIB | Any T | N3 | M0 |
| | T4 | Any N | M0 |
| Stage IV | Any T | Any N | M1 |

A help desk for specific questions about the TNM classification is available at http://www.uicc.org/tnm/

[#]The regional lymph nodes are the intrathoracic, scalene, and supraclavicular nodes.

**Figure 1-3: TNM Classification of lung tumors and Stage Grouping**

Malignant lung tumors can be classified by size (T1 - 4), number of tumor infected lymph nodes (N1 – 3) and whether or not distant metastasis occurred (M0 / M1). (Figure adopted from Travis William D., 2015).

SCLC (Figure 1-2), whose name is originated from the small cells with bare cytoplasm it consists of (Travis William D., 2015), has the worst prognosis of all lung cancer subtypes and is normally located in the central lung. As it has a very high tumor doubling rate, 80% of the cases are metastasized when diagnosed (Herold, 2017; Travis William D., 2015). Thus, SCLC is often categorized in disease stages - very limited disease (small tumor size and no metastasis), limited disease (greater tumor size and lymph node metastasis) and extensive disease (at least one metastatic lesion) (Collins et al., 2007; Herold, 2017).

The prognosis of NSCLC depends on the tumor subtype, tumor stage at time of diagnosis and the health status of the patient (Herold, 2017). Adenocarcinomas (Figure 1-2) and squamous cell carcinomas (Figure 1-2) have the highest

prevalence of all NSCLC subtypes. Adenocarcinomas, which are the most common malignant lung tumors among non-smokers, consist of a glandular structure and are more likely to develop in the periphery as seen in Figure 1-4 (Chen et al., 2014; Herold, 2017). They express a wide range of biomarkers, which can be detected via immunohistochemistry (IHC) such as Napsin A and thyroid transcription factor 1 (TTF1) (Chen et al., 2014; Osmani et al., 2017; Travis William D., 2015).

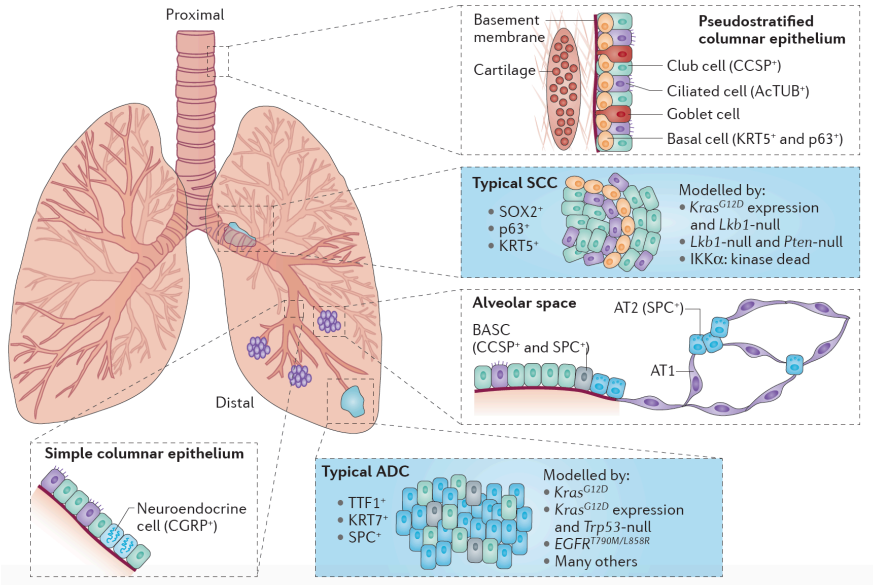


**Figure 1-4 Differences between NSCLC subtypes**

Squamous Cell Carcinoma (SCC) and Adenocellcarcinoma (ADC) develop in different areas of the lung and tumor growth is driven and modeled by different driver mutations. SCC arises from the pseudostratified columnar epithelium of proximal airways whereas ADC evolves in the distal lung. The tumor entities can be histologically differentiated by markers such as p63 and TTF1. (Figure adopted from Chen et al., 2014).

Squamous cell carcinomas (Figure 1-2), which are greatly associated with smoking, show a squamous differentiation and arise in the proximal regions of the air conducting pathways as presented in Figure 1-4 (Chen et al., 2014; Herold, 2017). They mostly express P40 and P63, cytokeratine 5 and 6 (CK5/6), as well as carcinoembryonic antigen (CEA). (Osmani et al., 2017; Travis William D., 2015). However, as IHC staining of biopsies is time and tissue consuming, triple markers combining staining for TFF1, Napsin A and P40 have been developed to distinguish the two main NSCLC subtypes. They show a higher sensitivity and

specificity than each marker alone and can be used with less biopsy material (Osmani et al., 2017). Furthermore, Adenosquamos carcinoma, Large cell carcinoma, Sarcomatoid carcinoma and also some carcinoid tumors are defined as NSCLC. However, because their prevalence is comparably low, they are not mentioned in greater detail here.

## 1.2 Lung cancer development

### 1.2.1 Basic principles of oncogenesis

In the developmental process of a tumor, cancerous and surrounding cells acquire distinct features facilitating tumor growth and metastasis. Through gaining genomic instability and mutations, tumor cells acquire the ability to sustain unlimited proliferation, to evade proliferation suppression, to resist cell death, to permit unlimited replicative cycles, to generate angiogenesis and to stimulate metastasis. In addition, they are able to deregulate their energetic system, to avoid destruction through immune cells and instead promote pro-tumorous inflammatory processes (Hanahan & Weinberg, 2000, 2011). However, not only cancer cells are responsible for the expansion of tumors but also stromal cells, such as fibroblasts, endothelial cells and immune cells, altogether being called the tumor microenvironment. As these cells are attracted and activated by the tumor, they turn from tumor suppressing to tumor promoting cell types, helping the tumor to grow, form pre-metastatic niches, invade surrounding tissue and suppress anti-tumor responses (Hanahan & Coussens, 2012; Hanahan & Weinberg, 2011; Quail & Joyce, 2013).

In the presence of cancer cells, vascular endothelial cells, for example, are activated through an “angiogenic switch” allowing them to form new vessels within the tumor and hence promote angiogenesis (Hanahan & Coussens, 2012). In addition, cancer associated fibroblasts are activated by growth factors and cytokines and transform into pro-tumorous cells and, for example, secrete extra cellular matrix (ECM) components or perform aerobic glycolysis. They thus provide the tumor with energy in form of lactate and pyruvate (Hanahan & Coussens, 2012; Quail & Joyce, 2013). Another important cell group in the tumor microenvironment are immune cells: Neutrophils, lymphocytes, monocytes, mast cells,

natural killer cells and macrophages can all be changed into pro-tumorigenic phenotypes by either being attracted by the tumor or by already being resident in the tumorous tissue site (Hanahan & Weinberg, 2011). They perform various tasks such as supplying growth factors (e.g. Epidermal growth factor (EGF), transforming growth factor beta (TGF-ß), fibroblast growth factor (FGF)), cytokines, interleukins, chemokines and histamine. In addition, they produce various proteolytic enzymes (e.g. metallo- and serine-proteinases), which can modify the extracellular matrix (ECM) and hence help the cancer cells to mobilize and form metastasis (Hanahan & Coussens, 2012). Further, myeloid-derived suppressor cells and regulatory T-cells can suppress anti-tumor responses for example by interrupting antigen presentation (Quail & Joyce, 2013).

Another distinct pro-tumorous cell type in the tumor microenvironment are tumor-associated macrophages (TAMs). TAMs influence tumor growth and progression as they, for example, promote angiogenesis by secreting high amounts of pro-angiogenic factors such as Vascular endothelial growth factor (VEGF) and growth factors such as EGF (Hanahan & Coussens, 2012; Noy & Pollard, 2014; Ostuni, Kratochvill, Murray, & Natoli, 2015). Another function is the promotion of cancer cell invasion and migration. TAMs modulate the ECM by production of proteases including matrix metalloproteinases (MMPs), which degrade the ECM and basement membranes and allow cancer cells to migrate to different sites (Qian & Pollard, 2010).

However, an additional mechanism that helps the tumor cells to escape the immune system works different than the pathways outlined above. In this case, it is not the tumor microenvironment that acts pro-tumorigenic, but cancer cells find a way to escape anti-tumor T-cell responses. They express a high amount of programmed death ligand 1 (PDL-1), a ligand that binds to the programmed cell death protein 1 (PD-1) on T-cells, inhibiting anti-tumor T-cell responses (Pardoll, 2012). Inhibiting this pathway as a therapy strategy has been investigated thoroughly in recent years (Langer, 2015).

### 1.2.2 Lung cancer driver mutations and lung cancer tumor microenvironment.

As mentioned above there are several different types of lung cancer and thus there are various driver mutations enabling tumor cells to perform the above mentioned features, thus promoting lung cancer development. Small cell lung cancer development for example is induced through mutations of p53, inactivation of the retinoblastoma gene or amplification of MYC (Travis William D., 2015).

However, NSCLC is driven by different genetic mutations. Very common genetic alterations in adenocarcinomas are, for example, TP53 mutations, K-ras mutations as well as epidermal growth factor receptor (EGFR) mutations and amplification (Blakely et al., 2017; The Cancer Genome Atlas Research, 2014). In addition, BRAF, MET, PIK3CA and others can be mutated (Chen et al., 2014; Hirsch, Suda, Wiens, & Bunn, 2016; The Cancer Genome Atlas Research, 2014). Furthermore, there is a high prevalence of co-occurrence of EGFR driver mutations with other genetic alterations for example mutations in MET, PIK3CA, MYC and CDK6. This co-occurrence of different genetic alterations might influence lung cancer therapy, especially targeted therapy approaches (Blakely et al., 2017).

Driver mutations in adenocarcinoma differ from those in squamous cell carcinoma, as genetic alterations in Lkb1, DDR2, FGFR1, FGFR2 and FGFR3 play a more important role. In addition, mutations in the PIK3 pathway as well as p53 mutations and others contribute to squamous cell carcinoma development (Figure 1-4) (Chen et al., 2014; Hirsch, Scagliotti, et al., 2016; Travis William D., 2015). Besides cancer cell heterogeneity in lung cancer, several publications suggest a diverse microenvironment in different NSCLC subsets. Pro-tumorigenic stromal cells, immune cells and endothelial cells can also be detected in the tumor microenvironment of lung cancer and fulfill functions as described above and shown in Figure 1-5 (Chen et al., 2014; Conway et al., 2016; Remark et al., 2015).

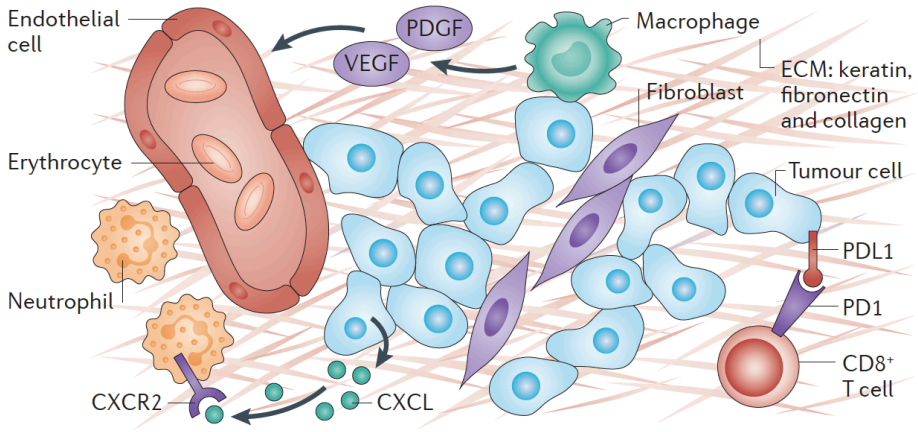


**Figure 1-5 Lung cancer microenvironment**

The lung cancer microenvironment consists of different cell types such as T-cells, neutrophils, fibroblasts and macrophages all helping the tumor grow and metastasis. Tumor-associated macrophages, for example, secret growth factors and ECM components. (Figure adopted from Chen et al., 2014)

B-cells, Natural killer cells, tumor-associated macrophages, neutrophils and others also interact with lung cancer cells through chemokines and interleukins and promote lung cancer development (Remark et al., 2015). Further, the PDL-1 and PD-1 Interaction described above and displayed in Figure 1-5 plays an important role in lung cancer and has fostered many new therapeutic strategies (Garon et al., 2015; Langer, 2015).

### 1.2.3 Tumor-associated macrophages in lung cancer

As mentioned above and shown in Figure 1-5, tumor-associated macrophages play an important role in cancer development. The presence of TAMs in the tumor microenvironment has been strongly associated with poor prognosis in several malignancies such as thyroid, breast and hepatic as well as lung cancer, especially NSCLC (Conway et al., 2016; Grivennikov, Greten, & Karin, 2010; Ostuni et al., 2015; Qian & Pollard, 2010). In addition, numerous studies have shown infiltration of TAMs in metastatic lesions in the lung, suggesting that they play a crucial role in the evolution of the pre-metastatic niche (Noy & Pollard, 2014). The effect of TAMs on lung cancer development is stressed by multiple studies, which show that depletion of macrophages in lung tumor models is followed by a reduction in tumor growth and metastasis rate (Ostuni et al., 2015; Qian & Pollard,

2010). However, contrary reports suggest that this depends on the localization of TAMs. They propose that TAMs localized in tumor islets and thus in between the tumor cells are correlated with higher survival rates in NSCLC patients and that TAMs localized around the tumor in the tumor stromal/microenvironment correlate with a poor prognosis (Conway et al., 2016; Remark et al., 2015).

TAMs typically arrive from circulating blood monocytes and are attracted to the tumor site by the chemokine CCL2, which binds to its receptor CCR2 on the macrophage surface (Ostuni et al., 2015). Once TAMs reach the tumor site, several growth factors such as colony stimulating factor (CSF1), granulocyte-macrophage colony stimulating factor (GM-CSF) and IL4 activate intracellular pathways programming them into a pro-tumorigenic phenotype (Noy & Pollard, 2014). In addition, VEGF, the chemokines CCL18 and CCL9 and interleukines IL3 and IL10 play a role in this process (Noy & Pollard, 2014; Ostuni et al., 2015; Qian & Pollard, 2010).

The CCL2-CCR2 axis plays an important role in the recruitment and function of TAMs in lung cancer and lung metastasis: the presence of CCL2 and CCR2 correlates with poor prognosis in lung cancer models and was detected in metastatic lesions in the lung of several cancer types (Ostuni et al., 2015; Qian & Pollard, 2010). Further, a preclinical approach of targeting the CCL2-CCR2 axis by antibodies against the chemokine showed a positive therapeutic effect as metastatic lesions in the lung decreased (Ostuni et al., 2015).

## 1.3 Lung cancer treatment

In general, lung cancer can be treated by three modalities – surgery, chemotherapy and radiotherapy, depending on the type of lung cancer, the stage at time of diagnosis and the individual receptor expression. Early stage (limited disease) SCLC can be treated by primary resection combined with radio- and chemotherapy. In this case, cisplatin and etoposide are the standard chemotherapeutics. However, when SCLC is, as it is mostly the case, detected in a late disease stage, primary palliative chemotherapy is the favored treatment option (Herold, 2017; Avrum Spira et al., 2015).

In the case of NSCLC, treatment options depend on the disease stage as well as on the individual receptor expression and molecular pattern of the tumor. The first line therapy of early stage NSCLC patients (stage I, II, IIIA) is the surgical resection of the tumor by lobectomy. Depending on the patient's comorbidity and age, a sublobar resection or a stereotactic ablative radiotherapy can also be chosen. In addition, patients may benefit from a perioperative chemotherapy or from chemotherapy in combination with thoracic radiotherapy (Herold, 2017; Avrum Spira et al., 2015). Adding Bevacizumab (anti-vascular endothelial growth factor antibody), however, showed no benefit in early stage NSCLC treatment (Hirsch, Scagliotti, et al., 2016; A. Spira et al., 2016).

Patients with advanced stage NSCLC may be eligible for targeted molecular therapies and therefore need to be tested before initiating treatment. If they do not meet the requirements for the approved molecular therapies, the first line therapy is a platinum-based doublet chemotherapy, which can be expanded with Bevacizumab if the tumor is not a squamous cell carcinoma (Herold, 2017; Hirsch, Scagliotti, et al., 2016). Nonetheless, if the NSCLC has a certain molecular profile, patients might be qualified for targeted therapy approaches. Several targeted therapies against oncogenic proteins in NSCLC have been approved such as against EGFR amplifications (e.g. Gefitinib, Erlotinib, Afatinib, Osimertinib), ALK- (e.g. Crizotinib, Alectinib) or ROS1- inhibitors (e.g. Crizotinib) and others are in phase two or three clinical trials (Herold, 2017; Hirsch, Scagliotti, et al., 2016; A. Spira et al., 2016).

As the tumor microenvironment plays an important role in NSCLC development, several treatment approaches of inhibiting TAMs and other immune cells have been developed. Novel therapies with anti-PD-1 antibodies Nivolumab or Pembrolizumab have been approved for metastatic NSCLC tumors after failure of the platinum based chemotherapy and others currently are in phase two or three clinical studies (Garon et al., 2015; Herold, 2017; A. Spira et al., 2016). Durvalumab, a PDL-1 Inhibitor, has recently shown positive results in a phase two clinical study with pretreated patients suffering from advanced non-small cell lung cancer (Garassino et al., 2018).

## 1.4 Nanoparticle-based drug delivery

### 1.4.1 Concept and advantages of nanotherapy

Nanoparticle-mediated drug delivery is an evolving therapeutic strategy in the field of cancer treatment. As conventional chemotherapeutics fail, challenges such as drug instability, short circulation time, unspecific targeting and increased side effects are of greater concern. Thus nanoparticle drug delivery systems, which are a broad range of therapeutic carrier systems, have been developed to address these problems (Torchilin, 2014).

Nanoparticles are nanometer sized (1-200 nm) particles, consisting of different materials, which can be loaded with or attached to a drug. As seen in Figure 1-6, there are particles containing a structure of organic material, such as proteins, carbon or carbohydrates and lipids and there are particles consisting of inorganic material such as metals or silica. In addition to their structure, their surface can be modified by adding targeting ligands, imaging or cell penetration agents (Torchilin, 2014; Wicki et al, 2014; Lammers et al, 2011). There are diverse types of nanoparticles including liposomes, micelles, metal nanoparticles, dendrimers, polymeric and mesoporous silica nanoparticles (Figure 1-6). Besides their use in cancer, nanoparticles are also used for imaging and for therapeutic approaches in other diseases such as cardiovascular disease and infections (Torchilin, 2014).

Common cancer targeting nanoparticle therapy approaches are “lipid based nanocarriers”, “polymer based nanocarriers”, “inorganic nanoparticles”, “viral nanoparticles” and “drug conjugates” (Wicki, Witzigmann, Balasubramanian, & Huwyler, 2015). These nanoparticles try to address the problems mentioned for common cancer therapeutics: They prolong circulation times, as they protect their cargo from enzymatic or non-enzymatic degradation and make therapeutics soluble. This protects them against renal clearance and therefore expands the bioavailability of the drugs (Lammers, Kiessling, Hennink, & Storm, 2012; Torchilin, 2014; Wicki et al., 2015).

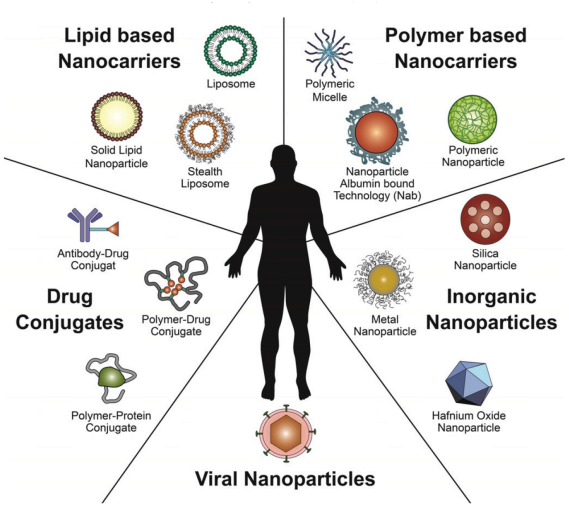


**Figure 1-6 Nanoparticle drug delivery systems**

Common nanoparticles used for drug delivery in cancer therapy. (Figure adopted from Wicki et al., 2015)

Further, nanoparticles can increase passive and active targeting of the drug. As tumors promote angiogenesis and enhance permeability of blood vessels, nanoparticles are transported to the tumor site to a greater extend than to other tissues and can leak to the tumor tissue through the permeable blood vessel structure. This is called the enhanced permeability and retention effect (EPR effect) and is responsible for an enhanced passive tumor targeting (Matsumura & Maeda, 1986). The first generation of nanomedicines for cancer primarily relied on passive targeting, using the EPR effect. However, this effect has some limits, as interstitial fluid pressure and heterogeneity of the tumor stromal can decrease the outcome and the particles can also be deposited in other organs with high blood supply (Lammers et al., 2012; Torchilin, 2014; Wicki et al., 2015). Thus, more potent targeting approaches have been developed. By conjugating nanoparticles with specific ligands, active targeting (Figure 1-7) of the tumor and/or surrounding cells can be achieved. By attaching a ligand or an antibody to the nanoparticle surface, which is directed to an overexpressed receptor on a cell (e.g. EGFR, HER2), the specific attachment of the nanoparticle to a cell type is possible and thus treatment is specific to this cell type (Lammers et al., 2012; Torchilin, 2014; Wicki et al., 2015).

In addition to the advances made in active targeting of nanotherapy, there has been improvement in the development of stimuli sensitive nanocarriers, as they

can be engineered to release their cargo upon specific stimuli such as acidic pH, hyperthermia, catalytic enzymes and hypoxia (Figure 1-7). Thus, nanoparticles can be developed that are only effective in certain tissues or areas, which again increases the targeting and reduces side effects (Lammers et al., 2012; Torchilin, 2014; Wicki et al., 2015). All of these functions can be combined, resulting, for example, in particles with a prolonged circulation time and targeting functions or particles that deliver multiple drugs at the same time and are stimuli-sensitive (Torchilin, 2014).

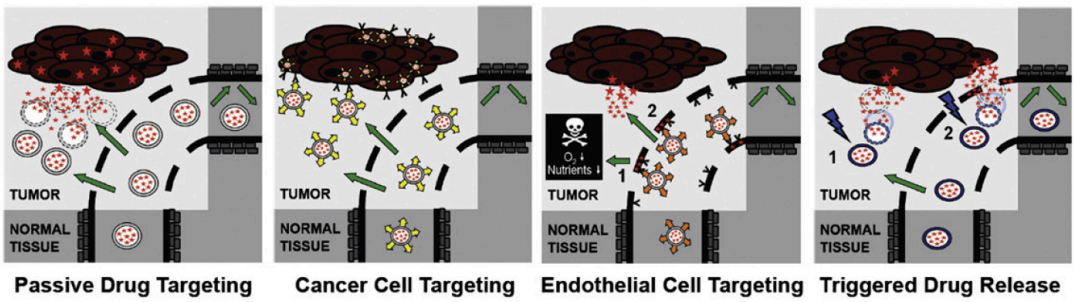


**Figure 1-7 Targeting mechanisms of nanoparticle drug delivery systems**

Nanoparticles can reach a target at the tumor site through different mechanisms. Passive targeting is achieved through a higher blood supply in the tumor and a higher permeability of the vessels. Active targeting, however, can be achieved by adding ligands to the nanoparticles and thus targeting structures on different tumor cell types such as cancer cells or endothelial cells. In addition, particles can be engineered to release their cargo in the presence of certain stimuli. (Figure adopted and modified from Lammers et al., 2012)

### 1.4.2 Nanotherapy in lung cancer

Among the groups of nanoparticles mentioned above, conjugated drugs have been the most successful systems in lung cancer therapy to date. They are drugs conjugated to targeting antibodies or ligands for prolonged circulation time and some have already been approved for clinical use. Among them is Abraxane, an albumin bound nanoparticle carrying Paclitaxel, which is also in use for NSCLC therapy (Bolukbas & Meiners, 2015; Wicki et al., 2015). Another nanotherapy for NSCLC, which was already approved in 2015, is a Paclitaxel loaded micelle (Genexol-PM). Besides these two approved drugs, there are several clinical trials for nanotherapies in lung cancer using for example liposomes, PEG-conjugation,

micelles and gold-silica nanoparticles (Bolukbas & Meiners, 2015; Landesman-Milo, Ramishetti, & Peer, 2015). Especially lipid based carrier systems have been developed, as they can encapsulate the drugs easily, are biocompatible and can be modified on their surfaces (Landesman-Milo et al., 2015). However, their low bio-stability and rapid renal clearance can be a problem (Yang & Yu, 2016).

So far lung cancer therapeutics have been delivered through intravenous or oral application. Another approach can be inhalation therapies as the local administration of the drug can potentially reduce side effects, decrease biodegradation and enhance cell-specific targeting. However, so far there are predominantly preclinical studies with antibody and cytotoxic drug delivery via inhalation, as concerns about occupational exposure, systemic effects and total lung toxicity have been raised (Abdelaziz et al., 2018; Kuzmov & Minko, 2015). In addition, local pulmonary clearance and lung specific side effects, such as high lung toxicity, impede inhalative approaches from entering clinical practice. Nonetheless, there is still a lack of clinical studies with inhalable nanoparticle formulations. As of yet only, a few lipid based approaches have been tested (Abdelaziz et al., 2018).

### 1.4.3 Mesoporous silica nanoparticles for nanotherapy

One of the evolving nanoparticles for targeted drug delivery and imaging approaches are mesoporous silica nanoparticles (MSNs). They consist of a silica core structure with various pores and can be formed in diverse morphologies such as spheres, hemi-spheres or dendritic structures. Further, their size and pore size can be altered according to the desired function (Yang & Yu, 2016).

A unique feature of MSNs is their porous structure, which can be sealed with different agents allowing a controlled release mechanism as seen in Figure 1-8 (Argyo, Weiss, Bräuchle, & Bein, 2014; Yang & Yu, 2016). In addition, MSNs are frequently used because of their ability to load a high amount of drugs, their high bio-stability and their relatively low cytotoxicity (Yang & Yu, 2016). Moreover, the surface of MSN can be easily modified: Ligands can be attached for specific targeting, gatekeepers for the pores can be introduced to allow a stimuli-sensitive release and coatings such as lipid layers, charged groups or polymers can be added for a higher bio-stability (Argyo et al., 2014).

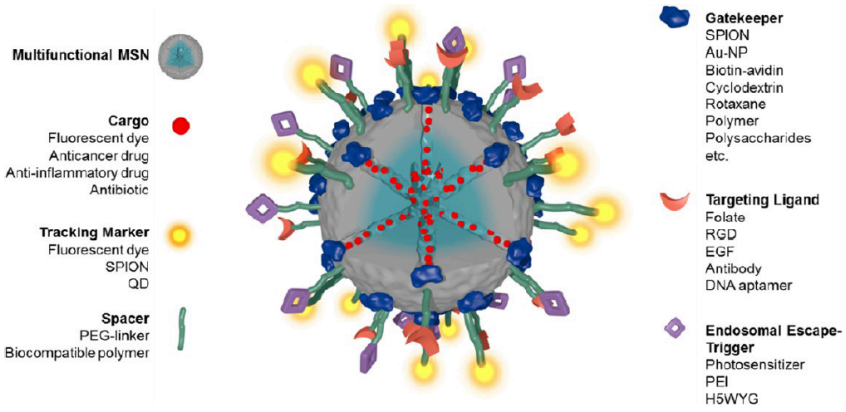


**Figure 1-8 Different possibilities of modifying Mesoporous Silica Nanopaticles**

The surface of MSNs can be modified through adding different ligands, gatekeepers, markers, spacers and triggers and thus targeting and cargo release mechanisms can be altered. In addition, different cargos can be packed inside the particle. (Figure adopted and modified from Argyo et al., 2014)

However, there are no clinical trials for NSCLC therapy approaches with MSNs and only a few preclinical studies have been published so far. In 2015, one phase one clinical trial has been started with gold-silica nanoshells and only a few preclinical studies with pure MSNs directed against EGFR overexpressing and luteinizing hormone releasing hormone receptor (LHRHR) overexpressing cells were initiated (Bolukbas & Meiners, 2015). Thus, there is still potential for developing MSN based therapy approaches for lung cancer.

# 2 Aim of the study

Lung cancer has one of the highest mortality rates of all cancers world-wide and as common chemotherapeutics fail to provide a promising effect, recent research has focused on new targeted therapeutic agents, which have shown to enhance cell specific toxicity while sparing healthy tissue. In addition, the focus has not only been on treating cancer cells but also on treating the lung cancer microenvironment, consisting of stromal and immune cells including tumor-associated macrophages (TAMs), that play an important role in the tumor initiation and development. In lung cancer, the chemokine receptor 2 (CCR2) is commonly overexpressed specifically on TAMs and cancer cells, thus targeting this receptor could be a valid strategy for a specific targeting therapy approach. So far, several targeted therapeutic agents for lung cancer against oncogenic proteins (e.g. *Erlotinib* or Afatinib) as well as against immune cell interactions (e.g. Pembrolizumab) have been approved. However, other options of targeting therapy approaches are nanoparticle-based carrier systems, among those are mesoporous silica nanoparticles (MSNs), as these can be modified to actively target specific cells. Accordingly, our idea was to functionalize a CCR2-targeting ligand on the surface of the MSNs to incorporate cell specific targeting for lung cancer treatment.

Therefore, the purpose of this study was to validate CCR2-targeted MSNs for lung cancer therapy and the aims were to test,

- whether CCR2-targeted MSNs are specifically taken up by CCR2 expressing cells *in vitro.*
- whether CCR2-targeted MSNs are preferentially taken up by CCR2 positive tumor cells and tumor-associated macrophages in a mouse model of lung cancer *ex vivo and in vivo*.

To this end, a CCR2 expressing cell line was used and CCR2-targeted MSNs were tested for their specific cellular uptake *in vitro* using confocal microscopy and flow cytometry analysis. 3D lung tissue cultures of wild type and K-ras mutant mice were used as an *ex vivo* model to observe specific uptake of the particles in tumor regions. In addition, an *in vivo* approach was conducted where the particles were locally applied to the lungs of K-ras mutant mice, to evaluate the biodistribution and specific tumor-targeting of the CCR2-targeted MSNs.

# 3 Materials and Methods

## 3.1 Materials

### 3.1.1 Antibodies

**Table 1: Primary antibodies**

| Antigen | Host | Application and Dilution | Supplier |
|---|---|---|---|
| CCR2 | Rabbit | IHC: 1:1000<br>WB: 1:1000<br>IF: 1:500 | Novusbio<br>(NB110-55674) |
| CD68 | Mouse | IF: 1:50 | Novusbio<br>(NBP1-74570) |
| β-Actin | Mouse | WB: 1:50000 | Cell Signaling (13E5) |

**Table 2: Secondary antibodies**

| Antibody | Host | Application and Dilution | Supplier |
|---|---|---|---|
| Alexa Flour 488 anti-rabbit | Goat | IF: 1:750 | Life technologies |
| Alex Flour 568 anti-rabbit | Goat | IF: 1:750 | Life technologies |
| Alexa Flour 488 anti-mouse | Goat | IF: 1:750 | Life technologies |
| Anti-Rabbit HRP-linked | Goat | WB: 1:40000 | Cell Signaling |
| Rabbit-on-Rodent AP-Polymer | | IHC | Zytomed |

### 3.1.2 Buffers and Solutions

**Table 3: Buffers for immunohistochemistry**

| Buffers | Reagents | Concentrations |
|---|---|---|
| Citrate buffer, pH 6 | Citric acid monohydrate<br>Sodium citrate tribasic | 1.8 mM<br>8.2 mM |
| TBS | Tris<br>NaCl | 24.2 g (0.242%)<br>80 g (0.8%) |
| TBST | TBS<br>Tween-20 | 1 x<br>0.0002% |

**Table 4: Buffers for immunoflorescence**

| Buffer | Reagents | Concentrations |
|---|---|---|
| PBS | NaCl<br>KCl<br>Na2HPO4<br>KH2PO4 | 137 mM<br>2.7 mM<br>10 mM<br>2 mM |

**Table 5: Buffers for flow cytometry**

| Buffer | Reagents | Concentrations |
|---|---|---|
| FACS-Buffer | PBS<br>FBS | 1 x<br>0.02% |
| FACS-Blocking buffer | PBS<br>BSA | 1 x<br>0.5% |

**Table 6: Buffers for DNA extraction**

| Buffer | Reagents | Concentrations |
|---|---|---|
| PBND | KCl | 50 mM |
| | Tris-HCL pH 8.3 | 10 mM |
| | MgCl2 | 2.5 mM |
| | Gelatin | 0.01% |
| | Nonidet P40 | 0.45% |
| | Tween | 0.45% |
| | H2O | |

**Table 7: Buffers for protein extraction**

| Buffer | Reagents | Concentrations |
|---|---|---|
| RIPA | Tris/HCL, ph7,5 | 50 mM |
| | NaCl | 150 mM |
| | NP40 | 1% |
| | Sodiumdeoxycholate | 0.5% |
| | SDS | 0.1% |
| | Complete© Protease Inhibitor | 1 x |

**Table 8: Buffers for Western Blot**

| Buffer | Reagents | Concentrations |
|---|---|---|
| Laemmli Buffer | Tris/HCL, pH 6,8 | 300 mM |
| | Glyercol | 60% |
| | SDS | 6% |
| | DTT | 5% |
| | Bromophenol blue | 0.01% |
| SDS-Page resolving gel (10%) | Tris/HCL, pH 8,8 | 375 mM |
| | SDA | 0.06% |
| | Acrylamide 30% | 10% |
| | APS | 0.125% |
| | TEMED | 15% |
| SDS-Page stacking gel (3,6%) | Tris/HCL, pH 6,8 | 125 mM |
| | SDS | 0.1% |
| | Acrylamide 30% | 3.6% |
| | APS | 0.125% |
| | TEMED | 0.3% |
| SDS-Page Running buffer | Tris | 25 mM |
| | Glycine | 0.192 M |
| | SDS | 0.1% |
| 10x SDS-Page transfer buffer | Tris | 25 mM |
| | Glycine | 0.192 M |
| | Methanol | 10% |
| PBST | PBS | 1 x |
| | Tween-20 | 1% |

### 3.1.3 Oligonucleotides

**Table 9: Primers for genotyping**

| Primer | Sequence |
|---|---|
| K-ras wildtype primer | 5'-TGCACAGCTTAGTGAGACCC-3' |
| K-ras common primer | 5'-GACTGCTCTCTTTCACCTCC-3' |
| K-ras mutant primer | 5'-GGAGCAAAGCTGCTATTGGC-3' |

### 3.1.4 Peptides

**Table 10: Ligands for MSNs**

| Name | Amino Acid Sequence | Supplier |
|---|---|---|
| ECL1 (C) | CKLFTGL | GenScript |
| Scrambled AS sequence | CTLLGFK | GenScript |

### 3.1.5 Cell culture

**Table 11: Cell lines and cell culture medium**

| Cell Line/Tissue | Culturing Media | Supplier | Supplements |
|---|---|---|---|
| A549 | DMEM | Life technologies | 10% FCS<br>1% Penicillin / Streptomycin |
| MHS | RPMI | Life technologies | 10%FCS<br>1% Penicillin / Streptomycin<br>1 mM Sodium-Pyruvate<br>10 mM HEPES<br>50 μM 2-ME |
| 3D-lung tissue cultures | DMEM/F12 | Life technologies | 10% FCS<br>1% Penicillin / Streptomycin<br>1% Amphotericin B |

### 3.1.6 Kits

**Table 12: Kits for different applications**

| KIT | Application | Supplier |
|---|---|---|
| BCA Kit | BCA | Thermo Scientific |
| Immunohistochemistry Kit (Vulcan fast red) | IHC | Zytomed |

### 3.1.7 Human tissue

Human tissue was kindly provided by the Asklepios Biobank for Lung Diseases, Gauting (project no. 333-10). Tumorous and tumor-free lung tissue from surgically treated lung cancer patients was used. All experiments with human tissue were approved by the Ethics Committee of the Ludwig-Maximilians-University Munich, Germany (LMU, project no. 455-12).

### 3.1.8 Chemicals

Chemicals were obtained from AppliChem, Sigma-Aldrich, Carl Roth, Roche and Thermo Fisher Scientific.

### 3.1.9 Consumables

Plastic ware and consumables were obtained from TPP, Greiner bio-one and Thermo Fisher Scientific.

## 3.2 Methods

### 3.2.1 Synthesis and characterization of nanoparticles

#### 3.2.1.1 Synthesis of mesoporous silica nanopartilces (MSNs)

Stefan Datz (Chemistry Department LMU, Group: Prof. Thomas Bein) synthesized the mesoporous silica nanoparticles at the chemistry department of the Ludwig-Maximilians University (Cauda, Schlossbauer, Kecht, Zurner, & Bein, 2009; Schlossbauer, Kecht, & Bein, 2009; Sabine H. van Rijt et al., 2015). The mesoporous silica nanoparticles were sealed with avidin and a pH-responsive linker. In addition, a ligand was attached for receptor-mediated uptake. For the CCR2-targeted MSNs, a CCR2-antagonist (ECL1 (C)) synthesized out of seven amino acids (Sequence: CKLFTGL) was used for the attached ligand (Auvynet et al., 2016). The antagonist was developed by Combadiere et al. (Patent Application US 2015/0011477 A1) and ordered through GenScript. The scrambled control particle was produced by attaching a peptide to the particles, which consists of the same amino acids as the antagonist but bound in a different order (Sequence: CTLLGFK).

#### 3.2.1.2 Dynamic light scattering and release experiment

Dynamic light scattering (DLS) measurements as well as the *in vitro* flourescine release experiments were kindly performed by Stefan Datz (Bein Lab, Physical Chemistry, LMU).

### 3.2.2 Cell culture

#### 3.2.2.1 Culturing of mammalian cells

For this thesis A549 and MHS cells were used. The cell lines were cultured in the appropriate media containing different nutritional factors and antibiotics (Table 11) and incubated at 37 °C with 5% CO2. Medium exchange with pre-warmed medium was performed 2-3 times a week according to the need of the cell line. When the cells reached around 80-90% confluency, they were sub-cultured in different ratios (1:10 – 1:2) depending on the growth rate and the subsequent

procedures. For detachment the cells were washed with PBS and a Trypsin-EDTA (0.25%) solution was added. Media with 10% fetal calf serum was added to stop the activity of Trypsin and the cells were divided and sub-cultured in new flasks. Cell lines were cultured until they reached passage 25.

#### 3.2.2.2 Treatment of alveolar macrophages with MSNs

CCR2-specific uptake of MSNs was first assessed using murine alveolar macrophages (MHS cells) *in vitro*. For treatment with different types of MSNs, the cells were seeded into different sized wells depending on the subsequent experiments. For immunofluorescence staining of the cells, cover slips were placed in a 12-well plate and 250 000 and 500 000 cells per well were seeded on top. For determining the MSNs uptake with flow cytometry 500 000 cells per well were put in 6-well plates.

Before seeding, the cells were washed, detached as described above and counted using a Neubauer chamber. After seeding, the cells were left in the incubator overnight. The next day, MSNs covalently labeled either with Atto 633 or Atto 488 fluorophores were added at a concentration of 50 µg in 1 mL cell culture media supplemented with 10% FCS and 1% penicillin/streptomycin and the cells were placed for an hour in the incubator for MSN uptake. Afterwards, before continuing with the different procedures, the treated cells were washed three times with ice-cold PBS, and one time with ice-cold NaCl solution (0.15 M, pH 3.0) and again three times with ice-cold PBS to completely wash off particles sticking to the cover slips or the cell membrane.

#### 3.2.2.3 Flow cytometry analysis

For assessing the uptake of MSNs with flow cytometry, cells were treated with the particles as described above. In this case, the particles were labeled covalently with the Atto 488 fluorophore and the uptake was measured by comparing the median fluorescent intensity of the cells treated with different MSNs. After washing, the cells were detached from the wells with cell scrapers and dissolved in FACS buffer containing 2% FCS. Flow cytometry analysis was performed using

the LSR II (BD Biosciences) and the fluorescent intensity was assessed. 10 000 cells were counted for each condition.

#### 3.2.2.4 Immunofluorescence staining

As another method for measuring the specific uptake of MSNs, immunofluorescence staining was used. For this procedure, MHS cells were incubated with MSNs labeled with Atto 633 for one hour. The cells were seeded on cover slips, treated and washed afterwards as described above. For fixing, they were incubated in 70% ethanol solution for five minutes. Depending on the purpose, the cells were stained with the appropriate antibody. In addition, cell nuclei were stained with DAPI and cytoplasmic actin was visualized with phalloidin.

In the former case, after the wash the cells were incubated with Roti-Immunoblock for one hour. This was followed by incubation with the primary antibody (Anti-CCR2 Antibody: 1:500 dilution) for one hour at room temperature or over-night at 4 °C. The secondary antibody was added in a 1:750 dilution and left again at room temperature for one hour. For counterstaining, DAPI and phalloidin were used. The cells were incubated with the DAPI/phalloidin mix (300 nM DAPI, phalloidin 1:300 dilution) for up to one hour and washed again afterwards. The cover slips were mounted on a microscopic slide using DAKO fluorescent mounting medium

For further assessment, confocal microscopy (LSM710 System, Zeiss) was used. Fluorescent intensity of the particles was measured and normalized to the fluorescent intensity of DAPI. Comparing the mean florescent intensity in the 633 channel of different treatment conditions assessed the specific uptake of MSNs per cell amount. Three sections on cover slips were chosen in a randomized manner and visualized with identical exposure times. Image processing was performed with the IMARIS software.

### 3.2.3 Protein extraction and analysis

#### 3.2.3.1 Protein extraction

To extract protein from cell lysates RIPA/Lysis buffer was used. Plated cells were washed with ice-cold PBS followed by addition of RIPA/Lysis buffer (with 1x complete protease inhibitor, 70 µl per well in a 6-well plate). The cells were then scraped off the dish, transferred into an Eppendorf tube and put on ice. For optimal protein extraction, the lysates were incubated on ice for 30 minutes and vortexed every 10 minutes. Cell debris was removed by centrifugation (14 000 RPM, 4 ˚C, 30 minutes), the supernatant was transferred to a new tube and stored at -20 ˚C for further analysis.

#### 3.2.3.2 Analysis of protein concentration

To determine the protein concentration in the lysates, a bicinchoninic acid assay (BCA) was performed using the Pierce BCA kit according to the manufacture's protocol. The samples were diluted 1:10 or 1:5 with PBS 25 µl of this mixture were put in a 96-well plate and 200 µl of the BCA solution provided by the kit was added per well. In addition, samples with a known protein concentration were assayed on the same plate to determine a standard curve for further calculations. After incubation at 37 ˚C for 30 minutes, the absorbance was measured at a wavelength of 562 nm with the Sunrise Plate Reader (Tecan).

#### 3.2.3.3 SDS-Page and Western Blot

For determining the CCR2 expression in the seeded cells, SDS- polyacrylamide gel electrophoresis (PAGE) and Western blotting was performed. For SDS-Page, Lämmli loading buffer was added to 10-20 µg of protein samples and the mixture was incubated at 95 ˚C for 10 minutes. The samples were loaded onto 10% SDS PAGE gels (1.5 mm thick) and the electrophoresis was run in running buffer at 90 V, which was increased to 110 V after the protein left the stacking gel.

After the electrophoresis, the gels were blotted on a methanol-activated PVDF membranes. Transfer buffer was added to the Mini Protean Tetra electrophoretic transfer cell and blotting was performed for 90 min at 200 mA. Afterwards the

membrane was blocked by incubating it for one hour in Roti Block. The primary antibody (CCR2, 1:1000 diluted) was incubated with the blot over night at 4 ˚C. After washing 3 times with PBST, the HRP labeled secondary antibody (Anti-Rabbit, diluted 1:40000) was added and left for one hour. For detection of the signal, ECL solution (GE Healthcare, Solution A and B 1:1) was added and the blots were developed in the ChemiDoc (ChemiDoc XRS+, Bio-Rad) or the Curix 60 developer (Agfa). β-Actin was used as a loading control. Densitometry was done with the Image Lab Software (Bio-Rad) and the signal was normalized to the loading control.

### 3.2.4 Animal experiments

All animal experiments were approved by the Regierungspräsidium Oberbayern and were performed by Deniz Bölükbas according to the ethical guidelines of the Helmholtz Zentrum Munich. The further analysis of the material was performed by Deniz Bölükbas and Charlotte Meyer-Schwickerath.

K-ras$^{tm3Tyj}$ mice with lung adenocarcinomas were purchased from Jackson Laboratory and were further bred in the institute's animal facilities. The animals were kept in a surrounding where constant temperature and humidity were maintained. Further, food and water access was given ad libitum.

#### 3.2.4.1 Genotyping

For genotyping of the newborn animals, tail cuts or ear clips were used. The material was lysed with PBND buffer and Proteinase K and heated up to 56°C while shaking with 1250 rpm for at least four hours. After spinning the lysate for two minutes with 13000 rpm in the centrifuge, 150 µl of the supernatant was put in a new Eppendorf tube and stored at 4 °C for further analysis. Subsequently, PCR analysis was performed with the reagents summarized in Table 13. To 42 µl of the PCR mix, 8 µl of DNA were added and the PCR cycle was performed in the Master Cycle as indicated in the table below (Table 14), repeating the cycle 35 times.

**Table 13: Components of the PCR mix**

| Component | Concentration | Amount for 50 µl |
|---|---|---|
| PCR buffer | 10 x | 5 µl |
| MgCl2 | 50 mM | 2 µl |
| Nucleotides | 10 mM | 1 µl |
| Wt Primer | 10 µM | 0.5 µl |
| Mut Primer | 10 µM | 1 µl |
| Common Primer | 10 µM | 0.5 µl |
| Taq-Polymerase | 5 U/µl | 0.25 µl |
| H2O | | 31.75 µl |

**Table 14: PCR cycle**

| Step | Temperature | Time |
|---|---|---|
| Denature | 94 °C | 1 min |
| Annealing | 60 °C | 2 min |
| Polymerase reaction | 72 °C | 1 min |

To determine the size of the gene product and distinguish between mutant and wild type animals, agarose gel electrophoresis was performed. For this purpose, 25 µl of the sample was mixed with DNA loading buffer and a gel electrophoresis in a 1.5% agarose gel containing 0.01% Sybr-safe was performed. The gel was imaged with the ChemiDoc (Gel imaging system ChemiDoc XRS+, Bio-Rad).

### 3.2.4.2 Hematoxylin and Eosin (H&E) staining

H&E staining was performed on paraffin sections prepared from the lungs of mutant or wild type mice. For this, the animals were narcotized with 100 mg/ml Ketamin and 0.7 mg/ml xylazine per kg body weight and opened with an abdominal cut. After exposure of the heart and the lungs, blood was taken with a syringe from the heart's left ventricle. The lungs were perfused with 0.9% sodium chloride solution and afterwards fixed by inflation with 4% PFA. Subsequently, they were withdrawn from the corps, fixed in 4% PFA at 4 °C overnight. Lungs were further processed in the tissue processor (Microtome STP 420D Tissue Processor) and embedded in paraffin. 3 µm thick slices were cut with the Hyrax M55 microtome (Zeiss), placed on microscopic glass slides and stored at 4 ˚C.

For staining of the sections, the paraffin was melted and subsequently removed by washing the slides in xylene and rehydrating them in different descending ethanol dilutions (100%, 90%, 80% and 70%). For H&E staining, the cuts were incubated with hematoxylin for six minutes, washed with tap water, incubated in 0.5% eosin G (containing 30 µL glacial acetic acid per 100 ml) for 10 minutes and washed with water again. To remove the excess reagent, the slides were washed with 80% ethanol and afterwards dehydrated by transferring them into 100% ethanol and 100% xylene. The slides were then mounted with Entellan (Merck Millipore) and imaged with the Mirax scanner (Zeiss). Image processing was performed with the Pannoramic viewer software (3DHISTECH).

### 3.2.4.3 Immunohistochemistry – paraffin cuts

For immunohistochemistry, the tissue was embedded in paraffin and sectioned as described above. Furthermore, the removal of paraffin was also performed as described for the H&E staining. After rehydration, the cuts were incubated in a 30% H2O2 and methanol solution for 20 min for membrane permeabilization and blocking of the endogenous peroxidase activity. Antigen retrieval was performed with citrate buffer (pH 6) and the slides were heated up to 125 °C for 30 seconds, followed by cooling down and washing steps with TBST for further cooling and neutralization. For the next steps, the slides were put into Shandon cover plates and were first incubated with Rodent Block M for one hour. Afterwards, the

primary antibody was added in the desired dilution (e.g., Anti-CCR2: 1:1000) followed by incubation with the Rabbit-on-Rodent polymer for another hour. The slides were incubated with AP substrate solution (Vulcan fast red) for 12 minutes and were finally counterstained hematoxylin. Excess reagent was removed by dipping the slides in 95% ethanol. Before mounting, the slides were dehydrated in different ascending solutions of ethanol and xylene (95% ethanol, 100% ethanol and 100% xylene). The slides were mounted and imaged as described for the H&E staining above.

#### 3.2.4.4 3D lung tissue cultures

For *ex vivo* 3D lung tissue cultures (3D-LTC), K-ras mutant or wild type animals were sacrificed as described above. After perfusing the lungs with 0.9% NaCl, the lungs were inflated with 1-2 ml of 2% agarose. The lungs were then resected from the corps and kept in DMEM/F12 media on ice until further processing.

For cutting the lungs into 300 µm thick slices, a vibratome (Hyrax V50, Zeiss) was used and the tissue cultures were incubated with DMEM/F12 containing 10% FCS, 1% P/S and 1% Amphotericin B for MSNs uptake analysis. For this purpose, the 3D-LTC were treated with different kinds of MSNs (50 µl/ml) labeled with Atto 633 and kept in the incubator for 12 hours. After washing three times with PBS, one time with NaCl pH 3 and three times with PBS, the lung slices were fixed with 70% Ethanol. After another wash with PBS, the tissue was stained with DAPI and phalloidin by incubating the slices in the solutions for one hour. This reaction was terminated by washing with PBS and mounting the slices onto microscopic slides with DAKO Fluorescent mounting medium. The uptake was measured with confocal microscopy by comparing the mean florescent signal in the 633 channel to the DAPI signal. For the K-ras mutated animals, three healthy and three tumorous regions per condition were selected in a randomized manner and imaged with the same acquisition settings. Image processing was performed with Imaris Software, Bitplane.

#### 3.2.4.5 Intratracheal administration of the MSNs

For assessing the bio-distribution of MSNs after application into the lungs, 50 µl of MSNs were intratracheally applied to the mice. For the procedure, the mice were narcotized by intraperitoneal administration of MMF (0.2 mg/ml Medetomidin, 2.0 mg/ml Midazolam, 0.02 mg/ml Fentanyl per kg body weight) and the particles were administered through a custom made tubus inserted through the trachea. After the instillation, narcosis was antagonized by giving 0.29 mg/ml Atipamezole, 0.059 mg/ml Fumazenil and 0.14 mg/ml Naloxone per kg body weight subcutaneously and the animals were monitored closely.

After three days, the animals were sacrificed and the organs were harvested as described above. The lungs were perfused with 0.9% sodium chloride solution and afterwards inflated with O.C.T. (Sakura – Tissue Teck) through the trachea. After the lungs were disconnected from the mice corpse, they were embedded in O.C.T and stored at -20 ˚C. The procedure was continued by harvesting the liver, kidney, spleen and brain.

#### 3.2.4.6 Immunofluorescence staining on cryosections

For evaluating the uptake of MSNs in the treated mice, all the organs were embedded in OCT, frozen in -20 ˚C and cut with the Hyrax C50 Cryotome (Zeiss) into 5 µm thick slices. For the lungs, each lobe was embedded and cut separately from the others.

The cuts were then fixed by incubating them in 70% ethanol and washed with PBS afterwards. For the first uptake analysis, DAPI and phalloidin were used to stain the tissue. For this, the slides were incubated for one hour with 300 nm DAPI and phalloidin (1:300 diluted) and again washed with PBS. For mounting of coverslips, DAKO fluorescent mounting medium was used and the slides stored at 4˚C protected from light.

As MSNs uptake in specific cells was analyzed, staining of cell receptors were prepared. For this, the sections were fixed by incubation in 4% PFA. They were afterwards washed with PBS + 0,1% Triton-X once, followed by two washes with pure PBS. For blocking they were incubated in RotiBlock with 5% Goat serum for 1.5 hours. The primary antibody (CCR2: 1:500; CD68 1:50) was left on the cuts

overnight, followed by the secondary in a dilution of 1:750. For counterstaining, DAPI and phalloidin were used as described above. The cuts were again mounted with DAKO fluorescent mounting medium and stored at 4°C.

The stained slides were imaged with the LSM imaging system (Zeiss), three pictures of each organ were taken in a randomized manner and the uptake was assessed by measuring the fluorescent intensity (Imaris Software, Bitplane) of Atto 633 (MSNs' signal) and normalizing it to the DAPI signal. For the lungs, three pictures of healthy regions and three pictures of tumor regions were taken per lung lobe.

### 3.2.5 H&E staining of human resections

Human tissue samples were kindly provided by the Asklepsios Biobank for Lung Diseases, Gauting, Germany. The obtained material was embedded in paraffin and sections were stained as described above in chapter 3.2.4.2.

### 3.2.6 Statistical analysis

For statistical analysis one sample t-tests were used. All statistical analysis was performed with the GraphPad Prism Software (Version 5). Significance was indicated as * $p<0.05$.

# 4 Results

## 4.1 Expression of CCR2 in human and mouse lung tissue

In order to confirm published expression data on CCR2 as a potential targeting receptor for nanoparticle mediated drug delivery, increased expression of CCR2 in primary human lung tumors and in the mouse model of K-ras-induced adenocarcinomas of the lung was validated.

### 4.1.1 CCR2 is overexpressed in human lung tumors

To confirm the overexpression of CCR2 in human lung adenocarcinomas, immunohistochemical staining of three human lung adenocarcinoma samples for CCR2 was performed. As seen in two representative stainings in Figure 4-1, indeed, tumor sections (A) showed an increase in CCR2 expression (red signal) in comparison to tumor free regions of the same patient's sample (B). Tumor free regions only showed a few positive cells in contrast to tumor regions where multiple positive cell clusters could be observed. In addition, a positive staining in the stromal cells around tumor cell nests was observed (A, Patient B). The negative control included an unspecific IgG antibody and proved specificity of the CCR2 staining. This indicates that the receptor might be a suitable target for future cell specific treatments as proposed before (Qian et al., 2011; Schmall et al., 2015; Wolf et al., 2012)

### 4.1.2 Tumors of K-ras mutant animals express CCR2

As an appropriate mouse model, the K-ras$^{tm3yj}$ mouse model from The Jackson Laboratory was evaluated, which shows early lung tumor development in 100% of the heterozygous animals (Johnson et al., 2001). As the tumor onset in this transgenic line develops by chance (Johnson et al., 2001) this mouse model mirrors the physiological condition in humans and represents the most appropriate transgenic lung cancer mouse model to date (Bolukbas & Meiners, 2015).

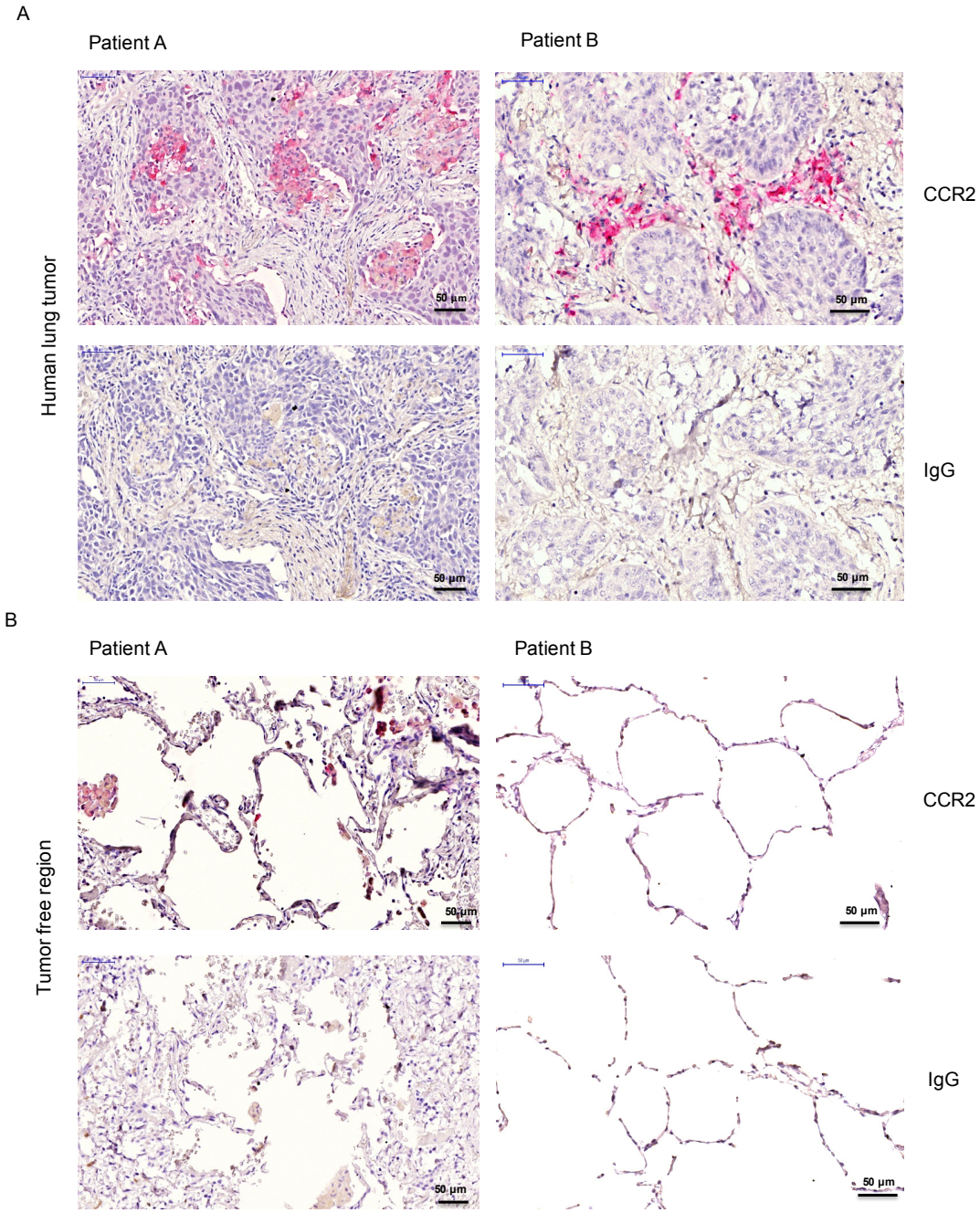


**Figure 4-1 CCR2 is overexpressed in human lung tumors**

A+B) Representative IHC staining of human lung tumors (A) and tumor free regions (B). Pictures of tumor and tumor free regions were chosen from two different patients. The slides were stained with an anti-CCR2 antibody (pink signal) and counterstained with hematoxylin. IgG Controls were performed to control for unspecific staining. n=3

To estimate tumor development and growth, paraffin embedded lung sections of 13 mice varying in age (6 weeks to 29 weeks) and gender (8 males and 5 females) were stained with Hematoxylin and Eosin. As the young animals (6 weeks after birth) already showed tumor lesions, an early onset of tumor growth can be

assumed. In addition, the pictures showed a heterogeneous tumor growth as the number of tumor lesions varied in between mice from the same age (Figure 4-2 B Nr. 154 and 155) and there was a high diversity in tumor size. This can be very well observed in mice Nr. 150 and 152 of Figure 4-2 B, as they have the same age but the size of the tumor lesions differs significantly.

A

| Mouse | Sex | Age (weeks) |
|---|---|---|
| 154 | Male | 6 |
| 155 | Male | 6 |
| 157 | Male | 6 |
| 161 | Female | 6 |
| 210 | Female | 6 |
| 202 | Female | 12 |
| 197 | Female | 16 |
| 150 | Male | 20 |
| 152 | Female | 20 |
| 189 | Male | 23 |
| 190 | Male | 23 |
| 143 | Male | 26 |
| 137 | Male | 29 |

B

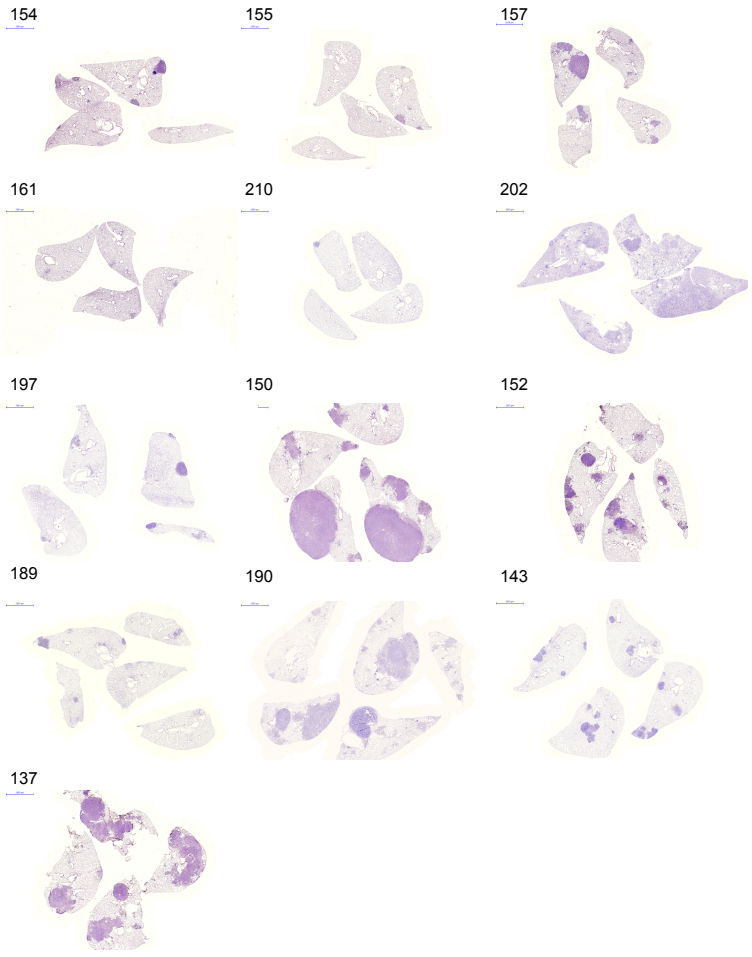


**Figure 4-2 Lung tumors from K-ras mutated mice differ in size and number**

A) Table with age and gender of K-ras mutated animals. B) Overview of HE stained lung sections of the different animals. Darker stained areas indicate tumor lesions. The pictures were kindly provided by Deniz A. Bölükbas.

To confirm overexpression of CCR2 in the tumors of the described mouse model, lung sections of K-ras mutated and wildtype mice were stained with an anti-CCR2 antibody. As shown in a representative section in Figure 4-3, tumors showed a clear signal in the cancerous areas, indicating an overexpression of CCR2 in tumors in comparison to tumor free regions and wild type animals. However, no

statement regarding the cell type expressing CCR2 could be made from the localization of the staining. CCR2 might therefore be expressed on cancer cells as well as on tumor stromal cells. Due to the positive CCR2 expression and the already named advantages of the mouse model, it was chosen for further experiments.

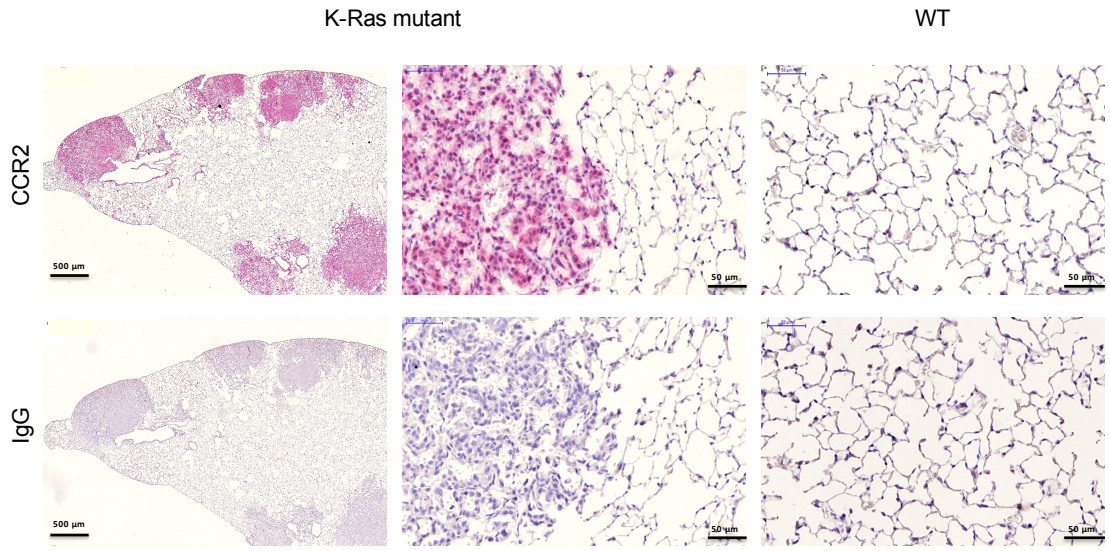


**Figure 4-3 CCR2 is overexpressed in lung tumors from K-ras mutated mice**

Fig: Representative IHC staining of K-ras mutant and wildtype lungs. The slides were stained with an anti-CCR2 antibody (pink signal) and counterstained with Hemalaun. IgG Controls were performed for each staining. K-ras mutant and wildtype lungs: n=3.

## 4.2 Synthesis and characterization of mesoporous silica nanoparticles

As CCR2 was overexpressed in human and mouse lung tumors, it was validated as an adequate target for cell-specific treatment. For this purpose, particles were designed to be taken up by cancer cells and tumor-associated macrophages through endocytosis and release their cargo inside the cell.

The particles used in this study consist of a SiO2 mesoporous core structure, which is sealed with the bulky avidin protein attached to the pore openings by a pH responsive linker (Cauda et al., 2009; Schlossbauer et al., 2009). In addition, a ligand for receptor-mediated uptake was added (Figure 4-4). In an acidic environment such as the endosomes, the pH-responsive linker is broken, the avidin caps are detached and the cargo can be released from the particle (Figure 4-4).

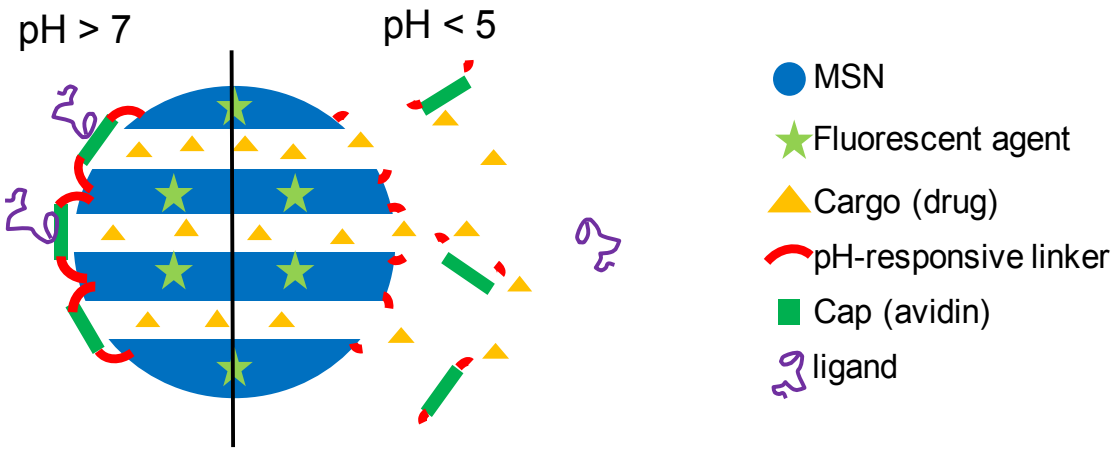


**Figure 4-4 Schematic representation of the CCR2-targeted MSNs**

The mesoporous silica nanoparticle (MSN) is sealed with an avidin cap (dark green) attached to a pH-responsive linker (red). A ligand (purple) is added for receptor-mediated cellular uptake. The particle can be loaded with a cargo (yellow) and labeled with a florescent agent (light green). Figure kindly provided by Deniz Bölükbas

### 4.2.1 CCR2-targeted MSNs and control particles do not differ in size

For the design of CCR2-targeted MSNs, a CCR2 antagonist (ECL1 (C) inverso) was used as a ligand (Auvynet et al., 2016). As controls, a non-targeted particle

(AVI) and a scrambled control particle, in which the ligand contains the same amino acids as the CCR2 antagonist but is arranged in a scrambled sequence, were chosen (Table 15).

**Table 15: MSNs used in the studies**

| Particle name | Ligand | Amino Acid Sequence of Ligand |
|---|---|---|
| AVI | No ligand | |
| CCR2-targeted | ECL1 (C) inverso | CKLFTGL |
| Scrambled control | Scrambled ECL1 (C) inverso | CTLLGFK |

To assess whether the particles show an increase in size when a ligand is added to the surface, a DLS measurement was performed. Figure 4-5 shows DLS measurement of two representative syntheses of AVI, CCR2-targeted and scrambled control particles. The majority of the particles were found to be similar in size differing between 90 nm and 200 nm, shown by the peek in the size curve. Thus adding a CCR2 ligand and a scrambled control ligand to the particle surface does not significantly increase the particle size.

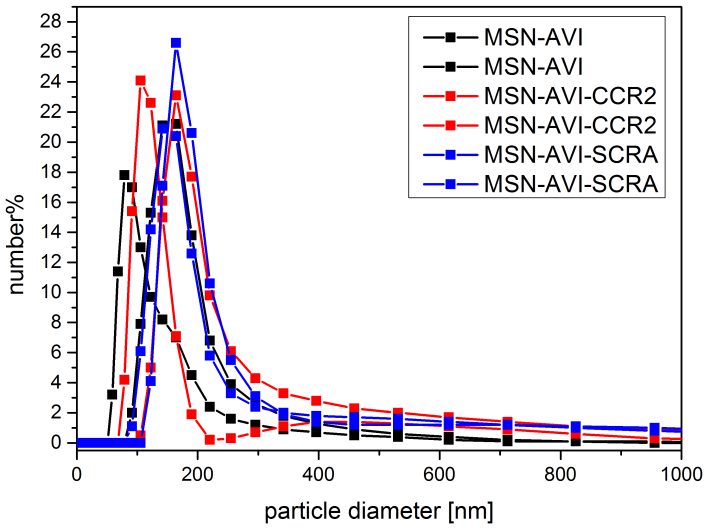


**Figure 4-5 MSNs are 90-200 nm in size**

DLS measurement of two representative particle syntheses of AVI, CCR2-targeted and scrambled control particles. The experiment was repeated 4 times in total. The measurement was performed and data was kindly provided by Stefan Datz.

### 4.2.2 MSNs release their cargo in an acidic environment

As the particles were sealed with a pH-responsive linker, cargo release was tested in response to different pH environments. This mechanism was tested by loading the particles with propidium iodide (PI) and measuring the absorbance at 500 nm wavelength of the surrounding solution depending on the pH. In the neutral environment (pH 7), the particles stayed sealed over 48 hours and PI was not released. However, when the surrounding pH dropped to 5, the particles were cleaved, PI was set free and the absorbance changed (Figure 4-6). In addition, the cleaving process increased over time with a maximum at 48 hours. As the pH found in the endosomal compartment after cellular uptake is acidic, the observed mechanism can be transferred to the cell leading to the assumption that the pH-responsive linker works similar releasing the particles' cargo after cellular uptake via endocytosis.

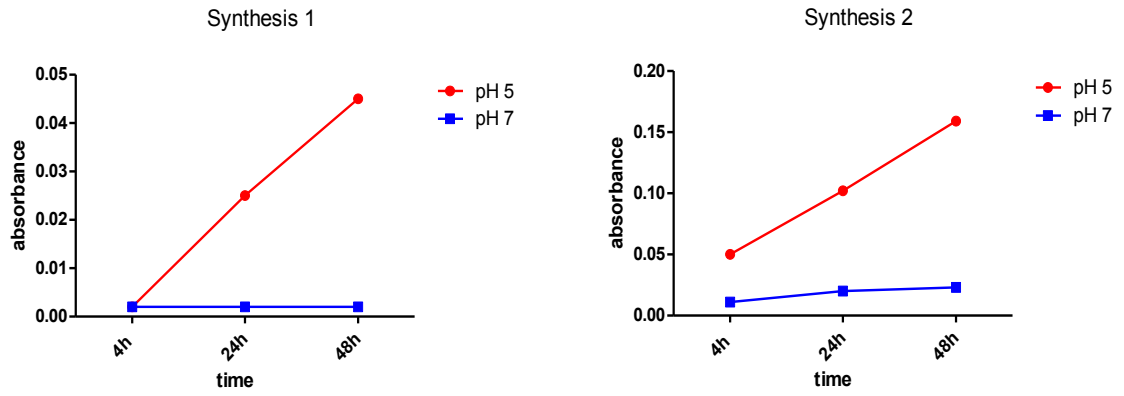


**Figure 4-6: CCR2-targted MSNs release their cargo in an acidic environment**

Particles were loaded with PI and absorbance at 500nm wavelength was measured, two representative syntheses are shown. The measurement was performed by Stefan Datz.

## 4.3 MSNs uptake by CCR2-expressing cells *in vitro*

As the synthesized particles showed a pH-responsive release of their cargo, the cell-specific uptake of CCR2-targeted MSNs was investigated. For this purpose, *in vitro* uptake experiments were performed in a suitable cell line that expressed high levels of CCR2.

### 4.3.1 MHS cells express CCR2

MHS, a murine alveolar macrophage cell line, mirrors alveolar macrophage function in the lung (Mbawuike & Herscowitz, 1989). CCR2 expression on MHS cells and A549 cells, a common lung cancer cell line (Giard et al., 1973), was investigated by Western blotting for CCR2. Detection of β-actin was used as a loading control. As seen in Figure 4-7 A and B, staining of MHS protein samples showed three distinct bands differing between 48 and 30 kDa in size, indicating two isoforms (two bands between 35 and 48kDa) and a glycolyzed form of CCR2 (Charo et al., 1994; Deshmane, Kremlev, Amini, & Sawaya, 2009). A549 cells showed a lower expression of CCR2 compared to MHS cells, which was validated by quantification of the signal relative to β-actin.

Immunofluorescence staining of MHS cells confirmed the expression of the receptor as a CCR2-specific staining was revealed on every cell (Figure 4-7 C). Image processing was performed to estimate whether the receptor is equally

distributed on the cell surface. The green signal represents the receptor, which showed a homogeneous distribution around the cell nuclei stained in blue (Figure 4-7 C). As these results indicated CCR2 expression on MHS cells, this cell line was used for subsequent uptake experiments.

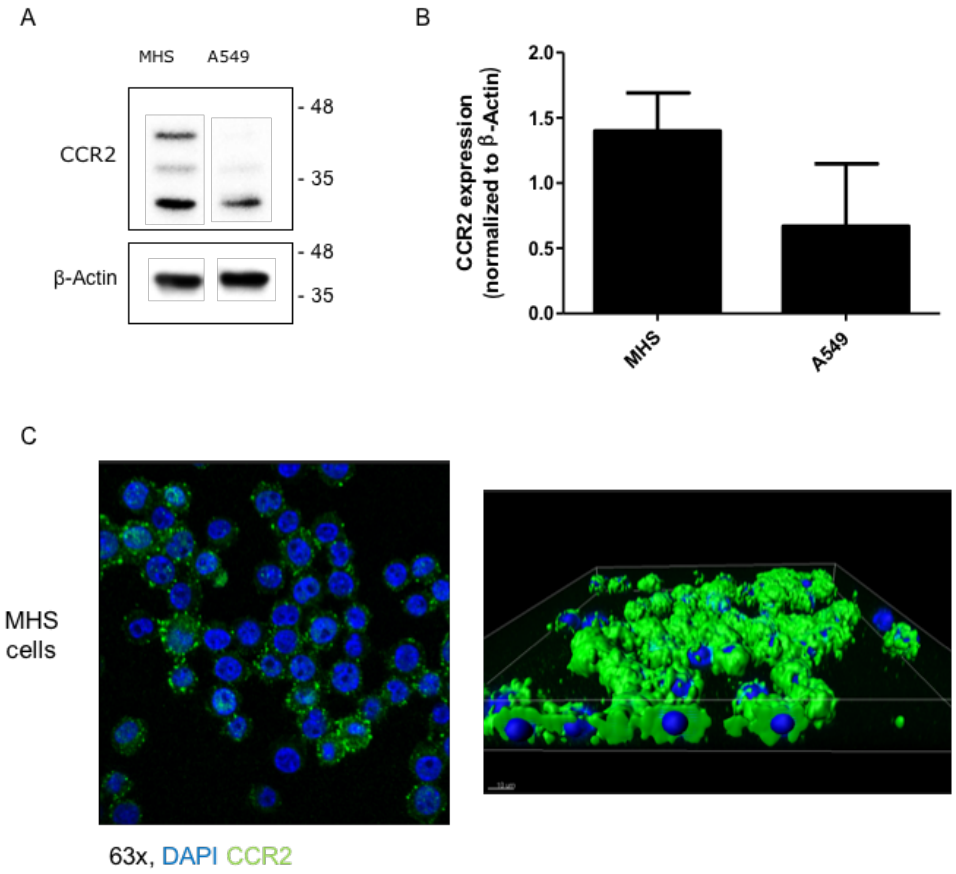


**Figure 4-7 MHS cells express CCR2**

A: Western blot analysis of CCR2 expression in MHS and A549 cells. Three different bands indicate two isoforms and a glycolyzed form (Charo et al., 1994; Deshmane et al., 2009). B: Quantification of Westernblot analysis, n=3 + SEM C: Representative IF staining of MHS cells for CCR2 receptor and image processing with Imaris software to show distribution of the signal, Picture was taken with 63x magnification.

### 4.3.2 CCR2-targeted MSNs are taken up by MHS cells

The first step was to evaluate the uptake of CCR2-targeted MSNs in comparison to scrambled control and AVI particles. MHS cells were treated with particles labeled with Atto 633 for one hour and were fixed and stained with DAPI and phalloidin afterwards. To avoid the detection of particles that unspecifically stick to

the cell surface, cells were extensively washed with PBS and NaCl pH 3 solution after the MSNs treatment.

As seen on the images in Figure 4-8 A, measured with confocal microscopy the fluorescence intensity of CCR2-targeted MSNs was higher than the signal of the control particles, which was also confirmed by quantification of the mean florescent intensity of each particle type (Figure 4-8 B). These results indicated a slightly higher uptake of CCR2-targeted particles in MHS cells compared to scrambled control and AVI particles (p = 0.0716).

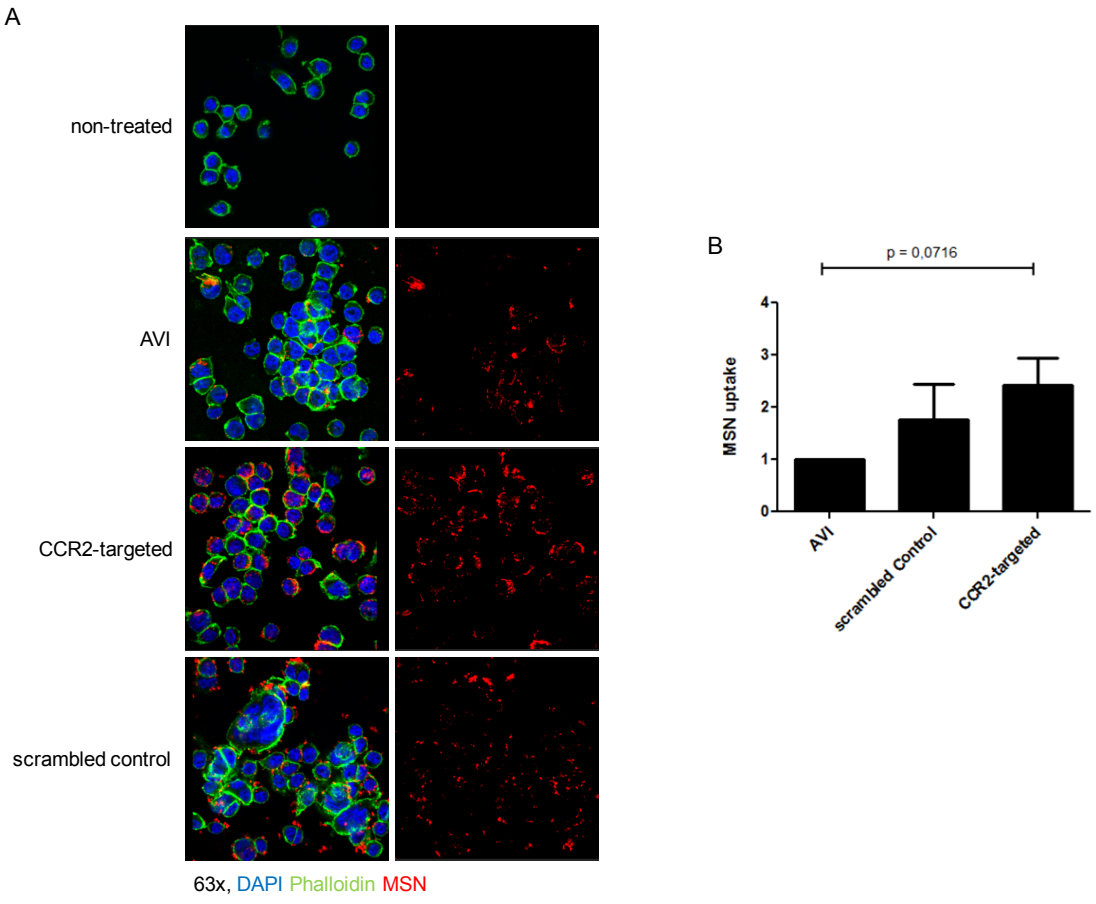


**Figure 4-8 Immunofluorescence staining: CCR2-targeted MSNs are taken up by MHS cells**

A: Representative immunofluorescence staining of MHS cells treated with MSNS. The images are taken with a 63x magnification. B: Quantification of MSN uptake measured with Imaris Software. Mean florescent intensity of the particles is normalized to mean florescent intensity of DAPI and the MSN uptake is normalized to AVI, n=4 (3 different particle syntheses, 4 different treatments) + SEM.

In addition, FACS analysis was performed to quantify the uptake using a second method. For this, MHS cells were treated with Atto 488 labeled particles for one hour and median fluorescent intensity was assessed. Indeed, previous results were confirmed as CCR2-targeted uptake was significantly ($p < 0.05$) increased (3.75 fold) in comparison to AVI particles and 9 fold in comparison to scrambled control particles (Figure 4-9).

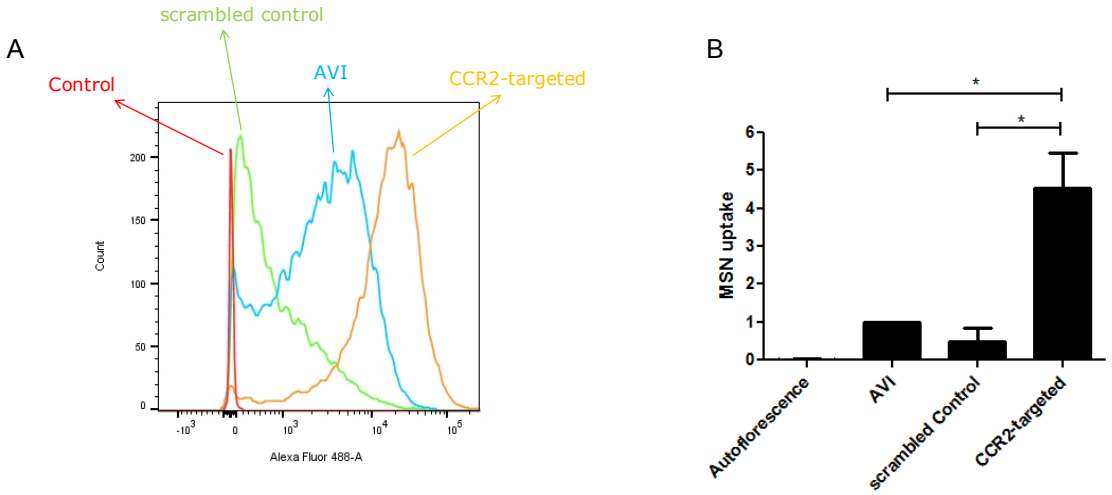


**Figure 4-9 Flow cytometry: CCR2-targeted MSNs are taken up by MHS cells**

A: flow cytometry analysis of MHS cells treated with MSNs, median florescent intensity of Alexa flour 488 was measured. B: Quantitative analysis of flow cytometry data, median fluorescent intensity was measured and normalized to AVI, * indicates $p<0.05$, n=4 + SEM.

When MHS cells, which had been treated with CCR2-targeted and scrambled control MSNs, were stained with an anti-CCR2 antibody an overlap of the receptor signal (green) and CCR2-targeted particle signal (red) was observed, indicating a co-localization and thus binding of the CCR2-targeted particle to the CCR2 receptor. However, this was also true for the scrambled control MSNs, therefore questioning a valid specific binding of CCR2-targeted MSNs to the receptor (Figure 4-10 A).

Nevertheless, image processing showed a homogeneous distribution of the CCR2-targeted MSNs around the cell nuclei and a close to complete uptake, as only few red particles stuck outside of the green signal, which was obtained by intracellular staining of the actin cytoskeleton with phalloidin (Figure 4-10 B). The

staining obtained with scrambled control particles, by contrast, revealed that these particles were mainly localized outside the cells in an area not stained with phalloidin or DAPI. They remained on the cell surface and in between the cells in greater numbers compared to the CCR2-targeted MSNs (Figure 4-10 C). This repeatedly indicated a more specific uptake of CCR2-targeted MSNs than of control particles.

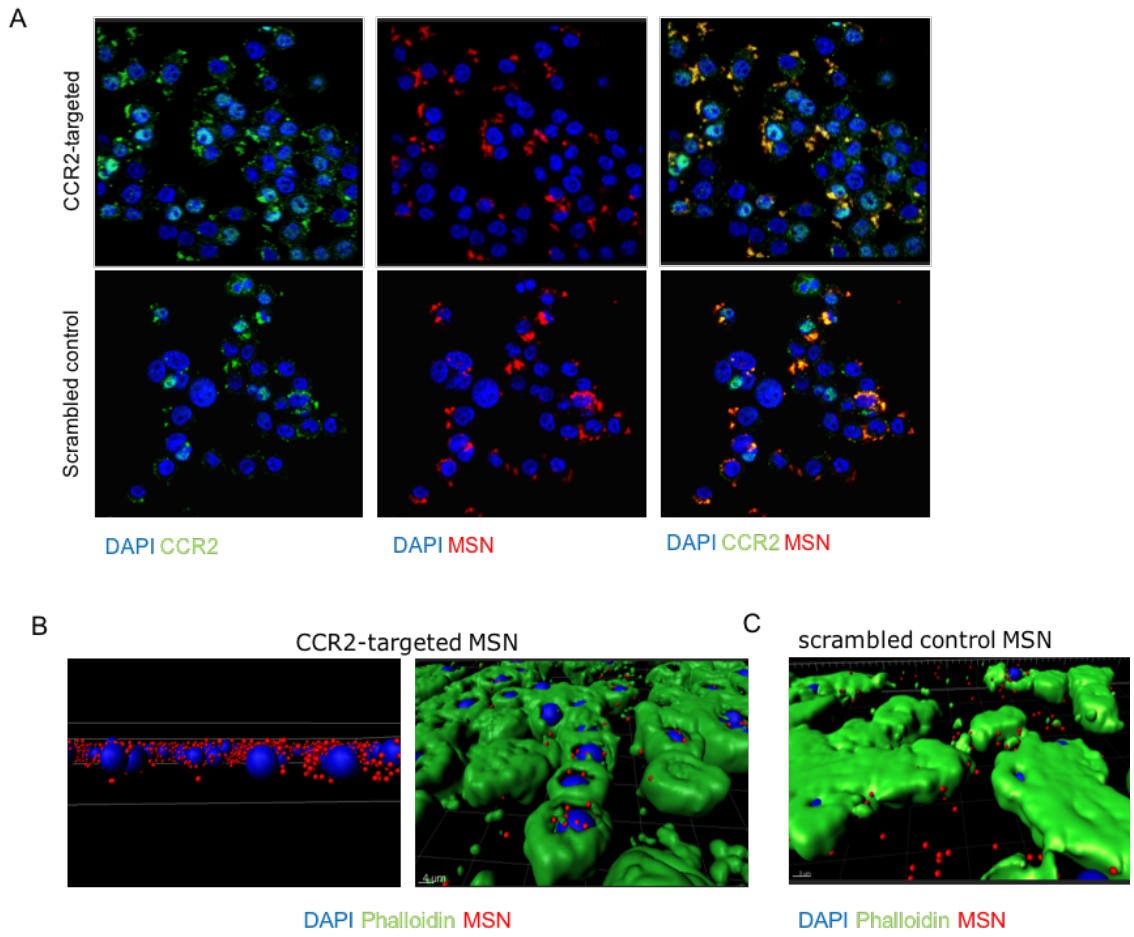


**Figure 4-10 CCR2-targeted and scrambled control MSNs co-localize with CCR2**

A: representative immunofluorescence staining of MHS cells treated with CCR2-targeted MSNs (red) or scrambled control MSNs (red) and stained for the CCR2-receptor (green). The images were taken with a 63x magnification. B+C: Image processing performed with the Imaris software. Blue spheres represent DAPI, green surfaces phalloidin and red spheres MSNS signal.

Concluding, *in vitro* experiments displayed cell specific uptake of CCR2-targeted MSNs in MHS cells. Targeted particles were taken up in greater number compared to AVI and scrambled control particles (Figure 4-8, Figure 4-9), showed a

co-localization with the CCR2 receptor (Figure 4-10) and were taken up into the cell as revealed by co-localization with the intracellular phalloidin signal (Figure 4-10). However, a specific binding to the CCR2-receptor is still questionable.

### 4.3.3 CCR2-targeted MSNs localize at a different part of the cell than AVI MSNs

The localization of AVI and CCR2-targeted MSNs on the cells was also investigated. Cells were simultaneously treated with both particles, which had been labeled with different florescent dyes, washed with PBS and NaCl pH 3 and stained with DAPI subsequently. As seen in Figure 4-11, AVI particles are distributed over the whole cell surface whereas CCR2-targeted MSNs seem to localize at specific spots on the cell surface. This leads to the assumption that the binding site and thus uptake site of the particle types differs depending on the presence of the CCR2 ligand.

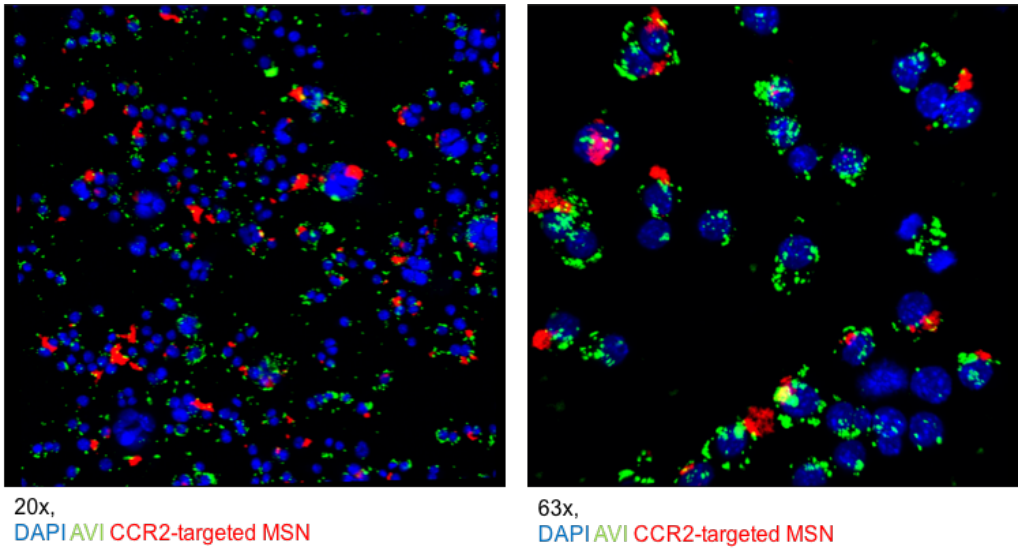


**Figure 4-11 CCR2-targeted MSNs localize to a different part of the cell than AVI MSNs**

Representative immunofluorescence staining of MHS cells treated with AVI (green) and CCR2 (red) targeted MSNs, experiments were repeated three times, three pictures of each microscopic slide were taken, one representative picture is shown. The images were taken with a 63x magnification.

## 4.4 MSN uptake in 3D lung tissue cultures

As it was shown *in vitro* that CCR2-targeted MSNs were taken up better than control particles by MHS cells, an *ex vivo* situation was used to test the particles in a more physiological condition. 3D lung tissue cultures (3D-LTC) are 300 to 500 µm thick slices of living lung tissue and can be held in culture for five days as cells remain viable and functional (Uhl et al., 2015). Therefore, these tissue cultures are an established *ex vivo* model for lung physiology and pathology. In addition, it has been shown that nanoparticles are taken up by the tissue in the 3D-LTC (Sabine H. van Rijt et al., 2015). Tumors of K-ras mutated animals show an increased expression of CCR2, which led to the idea of generating 3D-LTC of K-ras transgenic animals to test the targeted MSNs in an *ex vivo* situation. For this purpose, 300 µm think slices of lungs from K-ras mutant and wild type mice were incubated with CCR2-targeted and AVI MSNs for 12 hours and subsequently fixed and imaged for analysis.

### 4.4.1 Lung tumors in 3D lung tissue cultures of K-ras mutant animals do not show an increased uptake of CCR2-targeted MSNs

To assess preferential uptake of CCR2-targted MSNs by tumor cells and TAMs compared to healthy cells in order to analyze tumor-cell specific targeting, uptake of fluorescently labeled particles was monitored by confocal microscopy. Uptake of CCR2-targeted MSNs in K-ras mutant 3D-LTC was compared to uptake of AVI control particles in K-ras mutant 3D-LTC. For this purpose, the lung sections were incubated with the particles labeled with Atto 633 (red signal) for 12 hours and washed extensively with PBS and NaCl pH3 afterwards to discard excess particles. The sections where then counterstained with DAPI and phalloidin.

However, a difference of the particle signal between the tumor and tumor free regions in both particle types was not observed, indicating no uptake difference between the tumor and tumor free regions (Figure 4-12 A and B). Nonetheless, a difference in general uptake between CCR2-targeted and AVI control particles was observed. When comparing tumor-specific uptake of CCR2-targeted particles to tumor-specific uptake of AVI particles, a higher total signal of CCR2-

targeted particles was measured. This was also witnessed when comparing uptake in tumor free regions between the two particle types (Figure 4-12 A and B).

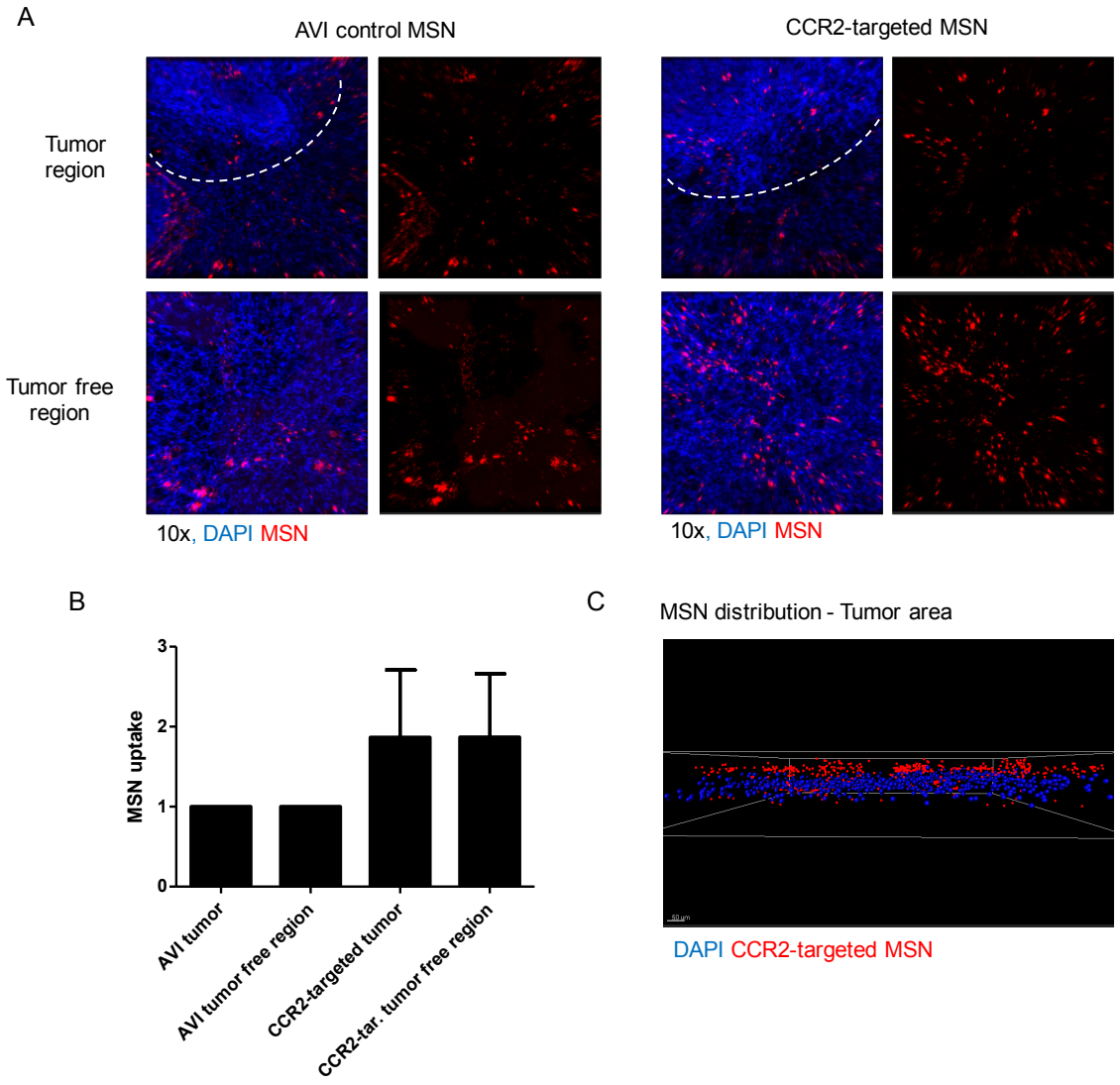


**Figure 4-12 Lung tumors in 3D-LTC of K-ras mutated animals do not show an increased uptake of CCR2-targeted MSNs**

A: representative pictures of tumor and tumor free areas of MSN treated 3D-LTC from K-ras mutant mice. The dashed line indicates the tumor. Pictures were taken with a 10x magnification. B: Quantitative analysis of MSN uptake in the tumor and tumor free region. Mean florescent signal of the particles is normalized to DAPI and the MSN uptake is normalized to AVI, n=3 (one particle synthesis, 3 treatments) + SEM. C: Image processing of K-ras mutant 3D-LTC treated with CCR2-targeted MSNs. Blue spheres represent DAPI, red spheres the MSN signal.

Yet, a limitation of the experiment was revealed when 3D scanning of the cultures via LSM showed that both particle types were more likely to stay on top of the lung slices and did not penetrate deeper regions (Figure 4-12 C) showing no penetration of the particles in the 3D-LTC. Thus it is questionable whether 3D-LTC are a suitable model for assessing targeted and non-targeted nanoparticle uptake in tumor models.

### 4.4.2 3D lung tissue cultures of wildtype animals show a reduced uptake of CCR2-targeted MSNs

The treatment of the K-ras mutant 3D-LTC showed a higher uptake of CCR2-targeted MSNs in general (in tumor and tumor free regions). To investigate whether this is due to the particle design or to a higher amount of CCR2 expressing cancer cells and tumor-associated macrophages, 3D-LTC of wild type animals were treated as described above. Strikingly, after washing the 3D-LTC, the signal of CCR2-targeted MSNs was decreased in comparison to the signal of AVI control particles in 3D-LTC of wild type animals (Figure 4-13 A and B). This might indicate a decreased uptake of the CCR2-targeted MSNs in comparison to AVI control particles, thus suggesting that the higher uptake in the 3D-LTC of K-ras mutant animals might be due to a higher density of CCR2-expressing tumor cells and macrophages in lungs of K-ras mutant animals.

However, AVI control particles seem to agglomerate more in the wt 3D-LTC (Figure 4-13 A and B) and once again it was observed that the particles were not equally distributed throughout the tissue culture but rather remained on the upper side (Figure 4-13 C) as described above for the K-ras mutant 3D-LTC. Hence, the mentioned problems with this *ex vivo* model led to the conclusion that 3D-LTC are not a valid model to assess differential uptake of cell-targeted nanoparticles.

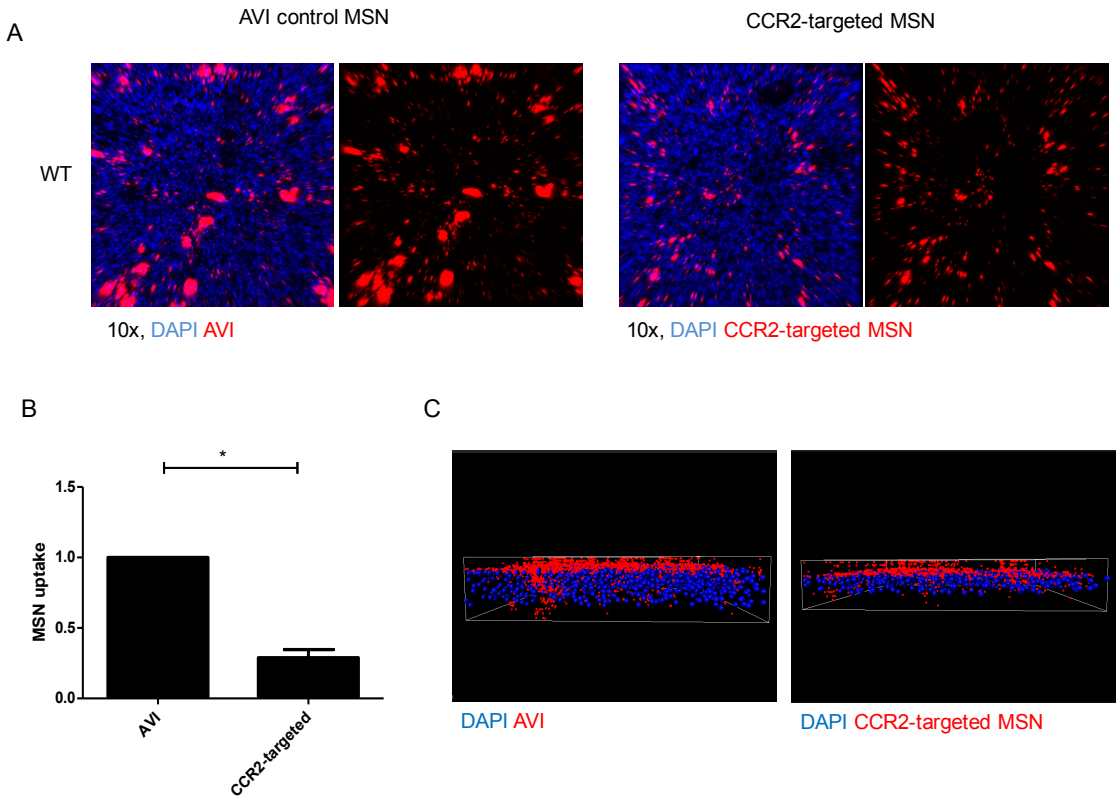


**Figure 4-13: 3D-LTC of wildtype animals show a decreased uptake of CCR2-targeted MSNs**

A: representative pictures of wildtype 3D-LTC treated with MSNs, pictures were taken with a 10x magnification. B: Quantification of MSN uptake in wildtype 3D-LTC. Mean florescent signal of the particles is normalized to DAPI and the MSN uptake is normalized to AVI, n=3 (one particle synthesis, 3 treatments) + SEM. C: Image processing with Imaris Software to show the particle distribution. The blue spheres represent DAPI, the red spheres the MSN signal.

## 4.5 MSNs uptake *in vivo*

To investigate the bio-distribution and uptake specificity of CCR2-targeted MSNs particles compared to control MSNs *in vivo*, we assessed differential uptake of the particles after local application into the lung. K-ras mutant animals were treated with a single administration of CCR2-targeted MSNs or AVI control particles, both labeled with Atto 633, through the trachea. After three days, the lungs, liver, spleen and kidney were harvested to evaluate the distribution of the applied MSNs and the uptake specificity (Figure 4-14).

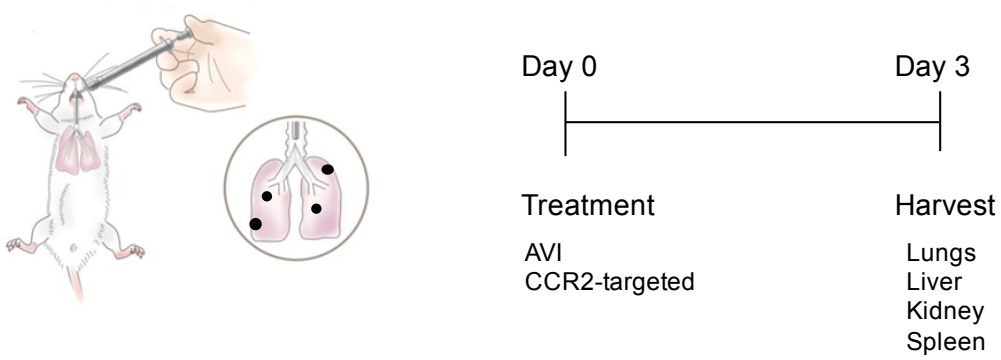


**Figure 4-14 Treatment scheme – Intratracheal administration of MSNs**

Edited from clodrosome.com/animal-injection

### 4.5.1 Intratracheally administered MSNs are not systemically distributed into peripheral organs

To evaluate whether CCR2-targeted and AVI control particles remain in the lung or enter the bloodstream and systemically distribute into peripheral organs, lungs, liver, spleen and kidney of each animal were examined. For this purpose, for each animal three cuts of each organ were stained with DAPI and phalloidin and subsequently pictures of three random sections of each cut were taken. As shown with a representative image in Figure 4-15, immunofluorescence signal of CCR2-targeted particles (red) and AVI control particles (red) was assessed and a pronounced signal was observed in the lungs compared to the other organs of the treated animals. This indicates no significant leakage/transport via the blood into other organs for both particle types (Figure 4-15).

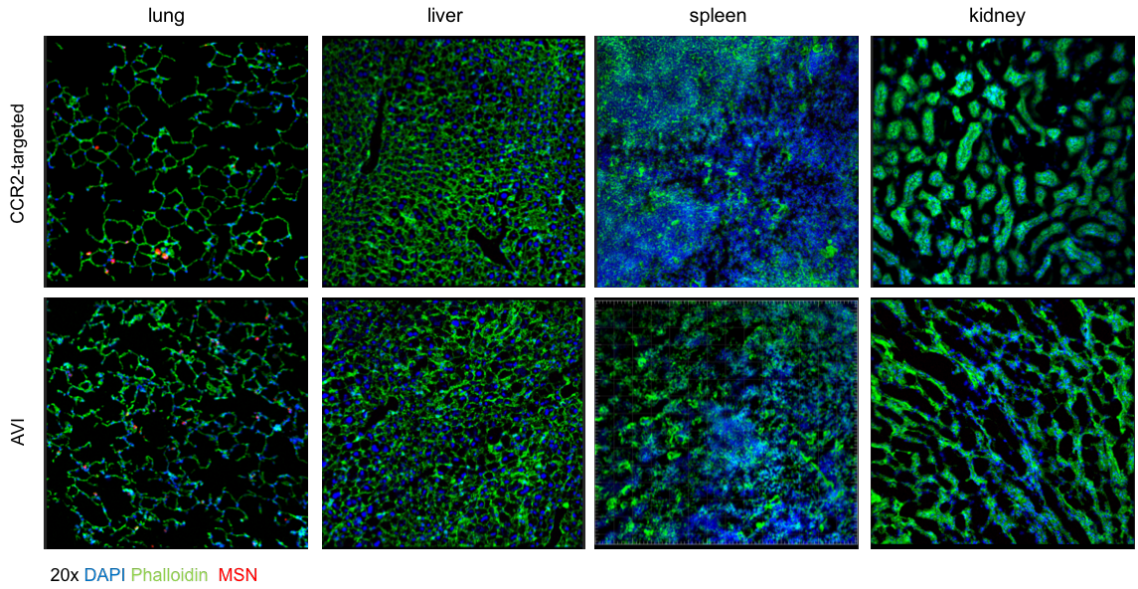


**Figure 4-15 MSNs do not significantly leak into the bloodstream when they are administered locally into the lung**

Representative IF staining of lungs, liver, spleen and kidney of K-ras mutant animals treated with AVI or CCR2-targeted MSNs. n=5, shown pictures were taken with a 20x magnification.

### 4.5.2 CCR2-targeted and control MSNs are taken up in the lung but show heterogeneous cellular distribution *in vivo*

For analyzing whether CCR2-targeted and AVI control MSNs reach all lung lobes and whether an active targeting could be observed, all lungs of the treated animals were dissected and cut into the five lobes. The lobes were then cut into 5 µm thick slices and three slices of each lobe were stained. Three random images of tumor and three random images of tumor free regions were taken and analyzed subsequently.

When analyzing the different lobes of each treated K-ras animal, it became obvious that the CCR2-targeted and AVI control MSNs reached all lung lobes, as nanoparticles were observed in alveoli of each lobe. In addition, MSNs were detected in tumor and tumor-free regions of the tissue. However, a heterogeneous distribution was observed as the density of the particles differed throughout the lobes of one lung and in between different animals (Figure 4-16).

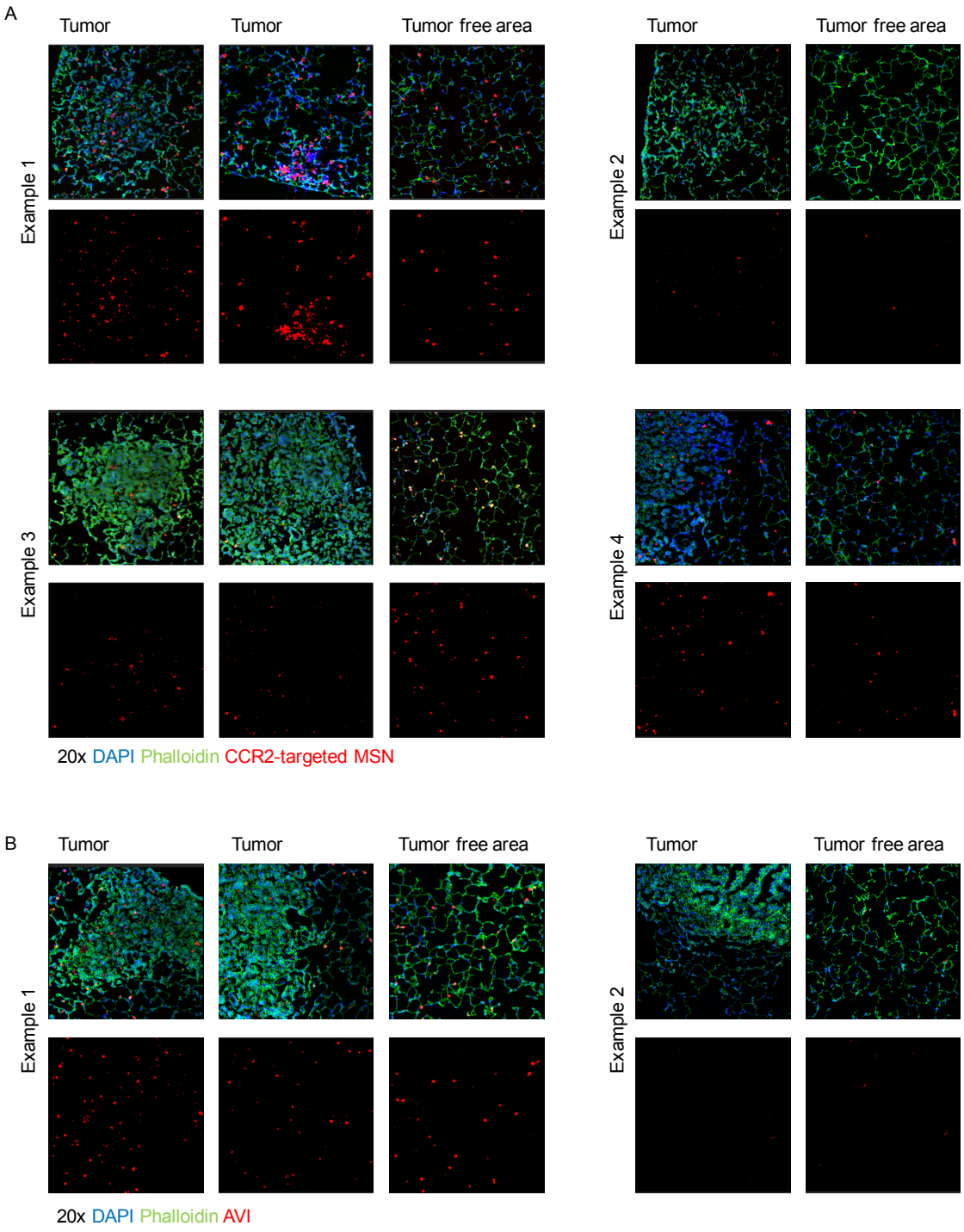


**Figure 4-16 MSN uptake into the lung of K-ras mutant mice is heterogeneous**

IF images of lungs from different K-ras mutant mice intratracheally treated with CCR2-targeted (A) or AVI control (B) MSNs. n=5 (For each group, 5 animals were treated, each lobe of the lungs was conserved and cut separately. Three pictures of tumor and three pictures of tumor-free regions were taken per mouse. For each example shown, pictures were chosen from the same lobe.) Images were taken with a 20x magnification.

Comparing the general uptake of CCR2-targeted to that of AVI control particles, no significant difference between the two types of MSNs could be observed (Figure 4-16 A and B). In addition, no trend in the differential uptake between tumorous and tumor free regions for each particle type could be validated (Figure 4-16). This indicates that the CCR2 targeting of cancer cells and tumor-associated macrophages does not improve tumor targeting specificity. CCR2-targeted MSNs are taken up in a similar manner as AVI control particles and do not specifically target tumors upon intratracheal instillation.

### 4.5.3 The uptake of CCR2-targeted and control MSNs *in vivo* varies between tumors depending on their size

Having a closer look on the images of tumor regions in the experimental setup describes above, it became obvious that CCR2-targeted particles are taken up better by small tumors in comparison to larger ones and that there is a higher uptake in the tumor edge regions (Figure 4-17 A). As this could also be detected for AVI control particles (Figure 4-17 B), it demonstrates that the specific targeting of K-ras mutant lung tumor cells with CCR2-targeted nanoparticles was not achieved. In general: tumor cells take up nanoparticles more avidly than healthy lung cells.

However, no quantitative analysis of the uptake could be performed, as the distribution of the particles in between the lobes and the lungs was too heterogeneous and there was no option to measure the tumor volume and size from a 2D picture and correlate this to the particle uptake. In addition, lungs varied in number and size of tumor tissue.

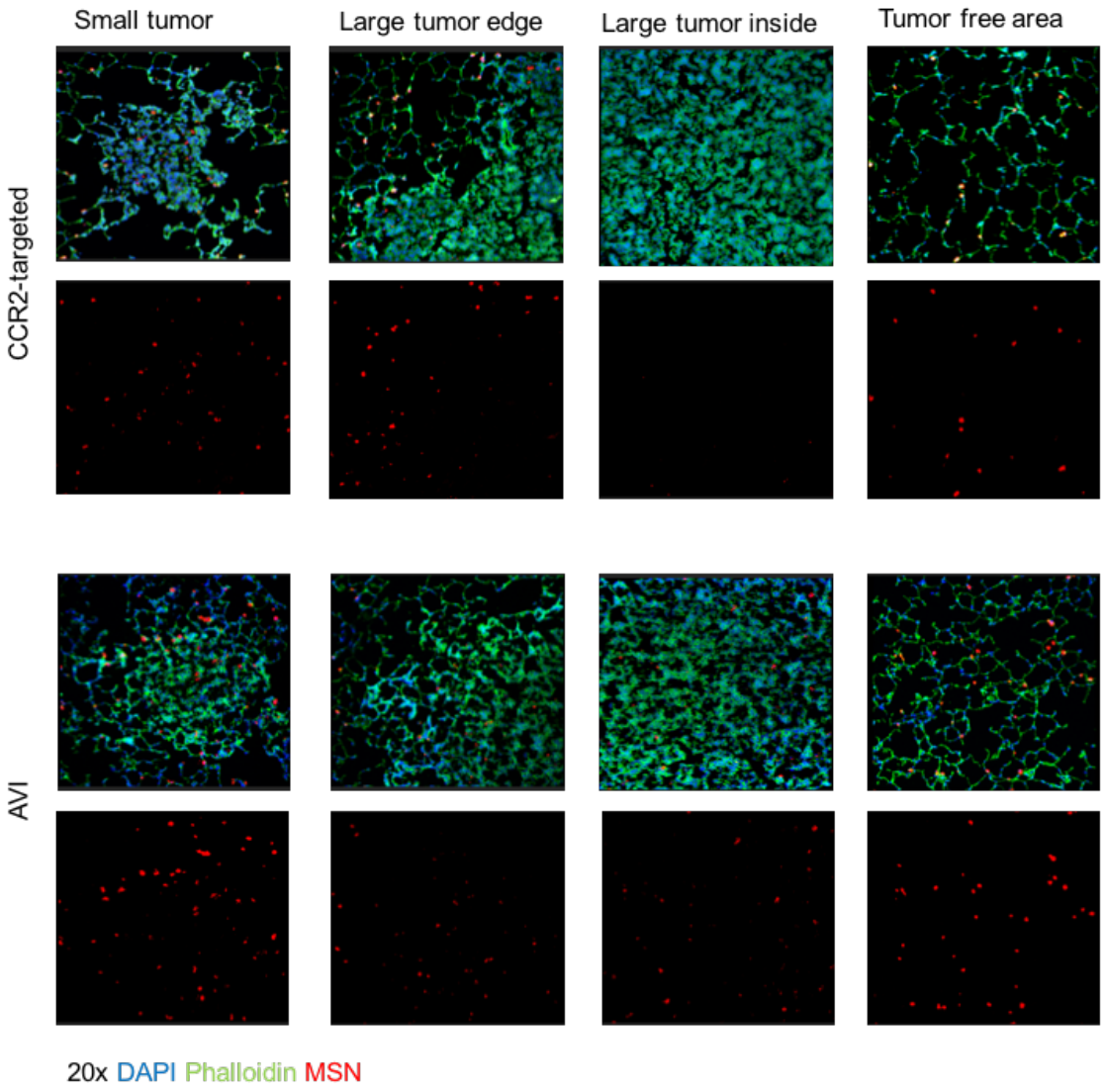


**Figure 4-17 Uptake of MSNs in lung tumors is dependent on tumor size**

Representative IF stained lung sections of K-ras mutant mice treated with MSNs intratracheally. Pictures are representative for three tumor regions from each mouse. For each treatment condition shown above pictures are chosen from the same lobe.

### 4.5.4 CCR2-targeted and AVI control MSNs are taken up by CCR2 positive cells in K-ras mutant mice when administered intratracheally

Even though tumor specific targeting with CCR2-targeted MSNs was not achieved, we wanted to evaluate whether CCR2-targeted MSNs are taken up specifically by CCR2-positive cells in tumor free regions. Therefore, three cuts of each lobe were stained for the CCR2 receptor, three random images of tumor free regions of each cut were taken and co-localization of the receptor signal and the Atto 633 labeled MSNs was evaluated.

The staining revealed a co-localization of CCR2-targeted Atto 633 labeled MSNs (white) and the CCR2 receptor (green) (Figure 4-18) in large cells situated in the alveolus on top of the endothelial cells. From the localization of these cells within the alveolus, it can be hypothesized that these cells are alveolar macrophages, phagocytic cells that take part in the pulmonary defense mechanisms (Welsch & Deller, 2014), which are positive for CCR2 staining in the lungs of K-ras mutant mice. Nonetheless, this co-localization of the CCR2-receptor (green) and the MSN signal (white) was also seen for AVI control particles in similar cells (Figure 4-18), indicating again a non-specific uptake of MSNs when given intratracheally to lungs of K-ras mutant mice.

### 4.5.5 CCR2-targeted and AVI MSNs are taken up in CD68 positive macrophages *in vivo*

To confirm the hypothesis that the MSN-phagocytosing cells mentioned above are alveolar macrophages, a staining of CD68, a marker for cells of the macrophage lineage including alveolar macrophages, was performed and co-localization with Atto 633 labeled MSNs was evaluated consecutively. For this purpose, again three cuts of each lobe were stained and images of three random tumor free regions were taken.

The staining supported the described cells as alveolar macrophages and revealed enhanced accumulation of MSNs in these cells in tumor free regions of intratracheally treated K-ras mutant lungs (Figure 4-19). However, this was not only true for CCR2-targeted MSNs but also for AVI control particles as demonstrated in Figure 4-19. In both treatment conditions co-localization of Atto 633

labeled MSNs (white) and CD68 receptor staining (green) was observed, indicating that both, CCR2 targeted and AVI control MSNs are taken up by the alveolar macrophages as part of their physiological foreign-body response function (Welsch & Deller, 2014).

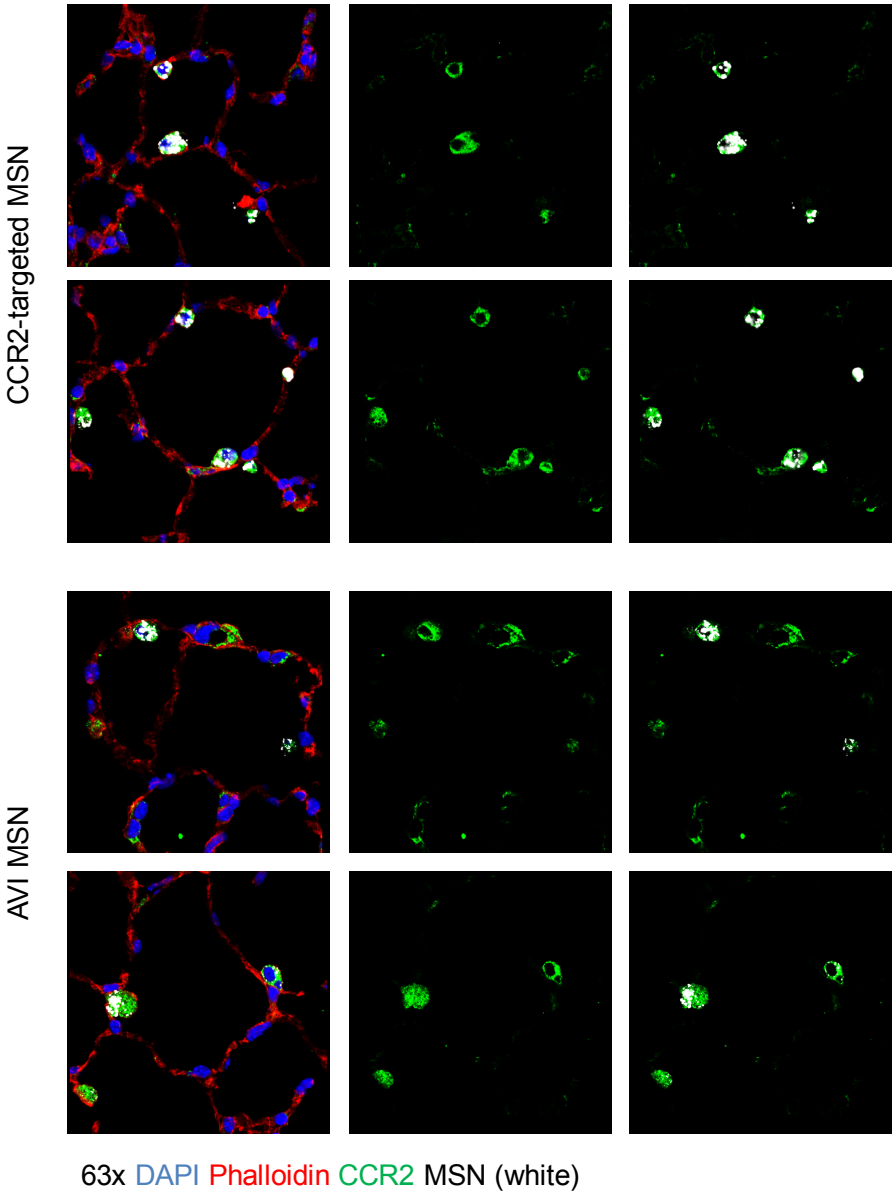


**Figure 4-18 CCR2-targeted and AVI control MSNs accumulate in CCR2 positive cells in lungs of K-ras mutant mice**

Representative IF staining for CCR2 in lungs of K-ras mutant mice treated with CCR2-targeted MSN or AVI control MSN intratracheally. n=4 (Lungs of four different mice for each treatment condition were stained and pictures of three different tumor free regions of each slide were taken.) Representative images are shown above. Images are taken with a 63x magnification.

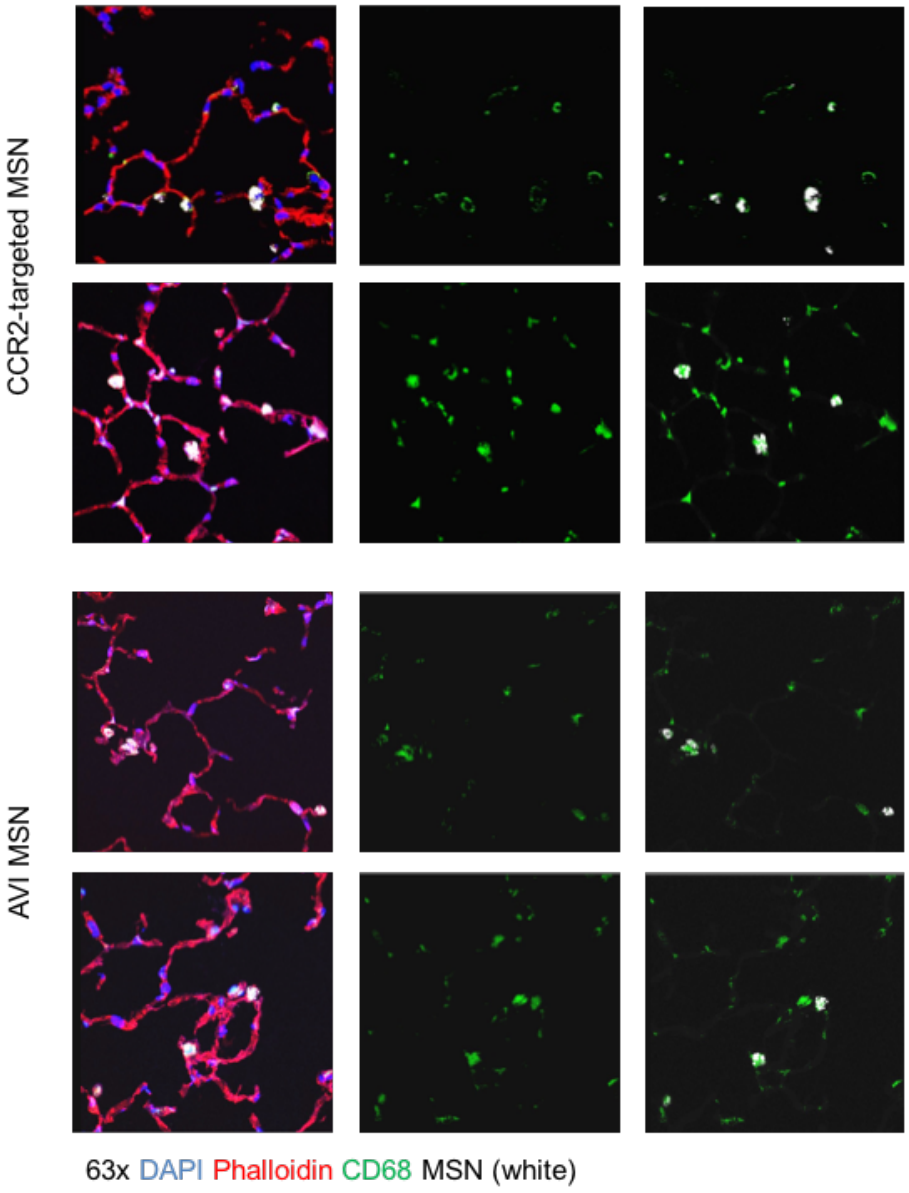


**Figure 4-19 CCR2-targeted and AVI control MSNs accumulate in CD68 positive macrophages in lungs of K-ras mutant mice**

Representative IF staining for CD68 positive cells in tumor free regions of K-ras mutant lungs treated with MSNs intratracheally. For each mouse (n=4), pictures of three different regions were taken and representative images are shown above. Images are taken with a 63x magnification.

*Data was obtained in collaboration with Deniz Bolükbas and was partly published in Bölükbaş, D. A. (2017). Development of novel nanoparticle-based therapeutics for treatment of lung cancer. München.*

# 5 Discussion

The aims of this thesis were to validate CCR2-targeted MSNs for lung cancer therapy by evaluating the cell specific uptake of CCR2-targeted MSN *in vitro* and in a lung cancer mouse model *in vivo*. In this context, first of all published data regarding the elevated expression of CCR2 in lung tumors was confirmed (Cortez-Retamozo et al.; Fridlender et al., 2011; Hiratsuka et al., 2013; Qian et al., 2011; Schmall et al., 2015) (Figure 4-1, Figure 4-3). In addition, this study provides *in vitro* proof-of-concept evidence that CCR2 can be used as a cell-specific receptor for targeted delivery of MSNs to CCR2 overexpressing cells as cell-specific targeting in an *in vitro* setup was successfully demonstrated (Figure 4-8, Figure 4-9). However, similar results could not be confirmed *in vivo*, as there was no increased cellular uptake of CCR2-targeted particles in lung tumors after local delivery of targeted nanoparticles to the lung (Figure 4-16, Figure 4-17). In contrast, alveolar macrophages were taking up targeted as well as non-targeted MSNs to a similar extent (Figure 4-19).

## 5.1 Discussion of experimental setup

### 5.1.1 Testing CCR2 targeted MSNs *in vitro*

When treating CCR2 expressing MHS cells with the synthesized MSNs we observed a higher uptake of CCR2-targeted particles than of AVI control or scrambled control particles. These findings were confirmed by confocal microscopy as well as FACS analysis (Figure 4-8, Figure 4-9). Interestingly, scrambled control particles were taken up by MHS cells in the FACS analysis experiments to a lesser degree than in the immunofluorescence staining experiments, which were assessed by confocal microscopy. As the incubation time and washing procedures were the same for both experimental setups, the technical procedures appear to play an important role. As stated above, scrambled control particles were observed to stick to the cell membrane to a greater extend and were not taken up in the same way as CCR2-targted MSNs (Figure 4-10). The measurement by confocal microscopy may have included these particles. We were only able to measure the complete signal of all particles on the slide and normalize this to our cell signal. Thus, particles localized next to cells may have been added to this

calculation. During the FACS analysis, these particles were not counted as only the overlay of the florescent signal of the particles with the florescent signal of the cell was measured and therefore free floating particles were excluded (Gottstein, Wu, Wong, & Zasadzinski, 2013). However, membrane bound particles were included in both experiments (Meindl, Öhlinger, Ober, Roblegg, & Fröhlich, 2017). In addition, due to technical reasons, FACS analysis can include a higher number of cells leading to more differentiated results (Gottstein et al., 2013; Meindl et al., 2017).

### 5.1.2 Testing CCR2-targeted MSNs *ex vivo*

Using the 3D lung tissue cultures (3D-LTC) as an ex vivo model for testing an active targeting nanotherapy approach revealed some complications. In the past, our group was able to translate this ex vivo model to tumor lungs of K-ras mutant mice and non-targeted stimuli-sensitive MSNs were successfully evaluated for their effectiveness (Sabine H. van Rijt et al., 2015). However, in the former experiments it already became obvious that MSNs are immobilized on top of the tissue and a deep penetration of the tumor is difficult to achieve in these settings (Sabine H. van Rijt et al., 2015). This was confirmed by our recent study for CCR2-targeted and control MSNs (Figure 4-12). Even though 3D-LTC are viable for at least five days and the organ structure is preserved (Uhl et al., 2015), the static condition of the experimental setup enhances particle aggregation, thus making it more difficult for the particles to diffuse into the tissue. In addition, the tumor tissue has a higher density and rigidity compared to the healthy alveolar tissue and the dense extracellular matrix impedes penetration of the particles (Jain & Stylianopoulos, 2010; Pickup, Mouw, & Weaver, 2014; Popović et al., 2010; Wilhelm et al., 2016). In the active targeting approach used here, the engineered nanoparticles need to be in direct contact with the target cell. Sufficient penetration of the tissue is thus a prerequisite for effective and cell-specific targeting. This differs from the study by Van Rijt et al., where MSNs, which release their cargo into the extracellular matrix by a secreted enzyme (MMP-9), were applied and deep penetration of the particles to the tumor was thus not necessary. In conclusion, 3D-LTC do not appear as a suitable model to assess cell-specific

targeting of CCR2-targeted MSNs due to inherent technical problems in tumor models.

### 5.1.3 Testing CCR2-targeted nanoparticles *in vivo*

Recently there has been a major debate about targeted nanoparticle therapy strategies failing to enter clinics. Among the reasons authors claim for this lack of translation of targeted therapies are the use of insufficient mouse models for precise *in vivo* testing of nanoparticle-based therapies and restriction of targeting by wrong administration of the nanoparticles (Bolukbas & Meiners, 2015; Lammers et al., 2012; Wilhelm et al., 2016). Accordingly, we designed an *in vivo* approach which addresses these shortcomings:

Many of the tumor models used for testing active nanoparticle-based targeting approaches do not represent the actual tumor development and physiology. Flank tumor models or lung metastasis models for example do not resemble the anatomical, biological and biochemical structure of lung cancer, thus a sufficient evaluation of a targeted therapy approach is hampered (Lammers et al., 2012; Wilhelm et al., 2016). In our study we addressed this problem by using the K-ras mutant mouse model giving a more physiological image of lung cancer development and constitution (Johnson et al., 2001). Hence, our experimental *in vivo* setup reduces misinterpretation of data and active targeting of the CCR2-targeting MSNs can be evaluated in detail.

In addition, unsuitable administration of the particles for the treatable tumor site is often regarded as another reason for the failure to translate targeted therapy approaches from bench to bedside. As an example, intra venous (i.v.) administration may not always be the fitting application route (Wilhelm et al., 2016). Cheng, Tietjen, Saucier-Sawyer, and Saltzman (2015) stress the importance of anatomically targeting the wanted organ to reduce unintended uptake of nanoparticles by bystander cells. We therefore used intratracheal delivery of CCR2-targeted MSNs to obtain maximal and local loading in our organ of interest, i.e. the lung. This approach has already been used by other preclinical and clinical studies resulting in lower systemic toxicity and higher accumulation of the therapeutic drug in the organ of choice (Mangal, Gao, Li, & Zhou, 2017; Zarogoulidis et al., 2012). Our data confirms the importance of a local delivery, as we did not observe

an enhanced systemic particle uptake in the spleen, liver or kidney, which has been an issue with many nanoparticle-based targeted therapy strategies before (Bertrand & Leroux, 2012; Yu & Zheng, 2015; Zhang, Poon, Tavares, McGilvray, & Chan, 2016).

However, one can not rule out local toxicity effects when giving nanoparticles directly into the lung, as previous studies showed an increase in acute and chronic lung damage such as bronchitis and bronchial wall thickening after inhalation of nanoparticles (Bolukbas & Meiners, 2015; Mangal et al., 2017; Zarogoulidis et al., 2012). Nonetheless the MSNs we used here did not induce any major inflammatory responses in previous studies of our lab (S. H. van Rijt et al., 2016), thus supporting the use of the intratracheal administration to enhance tumor-cell specific targeting.

## 5.2 Nanotherapeutic approaches need to be carefully validated *in vivo*

As mentioned above, we confirmed the cell-specific uptake of CCR2-targeted MSNs *in vitro* but failed to observe cell-specific targeting *in vivo*. In particular, when giving the nanoparticles intratracheally into the lungs of K-ras mutant mice, tumor-specific targeting of CCR2-targeted MSNs was not observed but alveolar macrophages encapsulated targeted as well as non-targeted MSNs to a similar extent (Figure 4-19). Our results stress the importance of evaluating targeted therapy strategies on a cellular level and not only total tissue uptake of nanoparticles, as the failure of the active targeting approach would have been missed. This accords well with previous claims for a more precise and detailed analysis of active targeting approaches on a cellular resolution level (Bolukbas & Meiners, 2015; Wilhelm et al., 2016).

Several causes could explain the failure of targeted delivery of CCR2-targeted MSN. As stated before, we reduced misinterpretation of data due to the fact that we used a valid lung cancer mouse model and enhanced tumor specific targeting by administering the MSNs directly to the lungs. However, we did not rule out impediment of the targeting approach by protein corona formation around the nanoparticles. As nanoparticles interact with proteins *in vivo*, previous studies

suggest this mechanism shields targeting ligands or enhances uptake of nanoparticles by phagocytic cells due to opsonizing of the particles by specific proteins (Salvati et al., 2013; Tenzer et al., 2013; Walkey et al., 2014). However, protein corona formation also occurs *in vitro* (Tenzer et al., 2013; Walkey et al., 2014), thus it does not fully explain the failure of the CCR-targeting MSNs approach *in vivo*.

Another reason for an insufficient active targeting therapy approach could be the choice of an inadequate target (Bolukbas & Meiners, 2015; Wilhelm et al., 2016). Nonetheless, we could confirm the overexpression (Figure 4-1) and thus potential targeting function of the CCR2 receptor in preclinical lung cancer models and human lung cancer samples (Cortez-Retamozo et al.; Fridlender et al., 2011; Hiratsuka et al., 2013; Qian et al., 2011; Schmall et al., 2015). Moreover, several studies have demonstrated that depletion and targeting of the CCR2 receptor reduces tumor growth in preclinical models of lung cancer, lung metastasis, lymphoma and pancreatic cancer (Fridlender et al., 2011; Leuschner et al., 2011; Marazioti & Stathopoulos, 2014; Mitchem et al., 2013; Roblek et al., 2016). Hence, the used receptor can be regarded as a suitable target for the nanoparticle-based therapy approach.

In addition, satisfactory tumor targeting can be restricted by high intratumoral pressure (Heldin, Rubin, Pietras, & Östman, 2004) and extracellular matrix conformation hindering particle penetration of the tumor (Cheng et al., 2015; Jain & Stylianopoulos, 2010; Nichols, Sakurai, Harashima, & Bae, 2017). While this is not a specific limit to an active targeting approach, our data indicates that our MSNs indeed only insufficiently penetrated dense tumor tissue while being able to reach smaller and less dense tumor lesions (Figure 4-17), in which intratumoral pressure end extracellular matrix formulation may not be fully developed.

Further, the clearance of nanoparticles by alveolar macrophages can restrict sufficient tumor targeting when administering targeting particles directly to the lung (Chung et al., 2017; S. H. van Rijt et al., 2016; Woods et al., 2015). Inhalative lung cancer therapy induces alveolar macrophage phagocytic responses and increases their number in the local tissue, thus enhancing nanoparticle clearance (Forbes et al., 2014). Our data emphasizes the clearing role of alveolar macrophages in nanoparticle-based therapy strategies for lung cancer. As our targeted

and non-targeted particles were taken up by these phagocytic cells to a similar high extent, a receptor mediated uptake of CCR2-targeted nanoparticles can be ruled out. Further, alveolar macrophages incorporated a high number of MSNs, giving the impression of this being the predominant up-taking cell line.

However, recent studies suggest using these properties of macrophages to efficiently target the tumor. They propose loading macrophages with drug-carrying nanoparticles and taking advantage of their ability to migrate deeper into the tumor tissue, thus transporting the therapeutics to the target site (Andón et al., 2017). In addition, re-educating tumor-associated macrophages or inhibiting TAM-recruitment to the tumor with the help of nanoparticles are also current research topics (Andón et al., 2017). In conclusion, these ideas are showing a possible use of the phagocytic function of macrophages for future tumor targeting strategies.

# 6 Conclusion

Evaluation of the CCR2-targeted mesoporous silica nanoparticles for lung cancer therapy revealed some distinct features. Firstly, the importance of the CCR2 receptor in lung cancer and the possibility of this receptor to act as a target for nanoparticle-based therapies was confirmed. Secondly, a clear difference in the results of the *in vitro* and *ex vivo* experimental setup was observed. While the targeted therapy approach was validated *in vitro*, the targeting capacity was lost in the *in vivo* approach. Thus, our study emphasizes the importance of a clear evaluation of targeted therapies on a cellular level, as the loss of targeting specificity became only evident when having a closer look at the up-taking cells *in vivo*. Our study stresses the function of alveolar macrophages in the clearance process of nanoparticles delivered directly to the lung. This function should be further analyzed in the future, as it can also be used for treating tumor-associated macrophages or other diseases in which macrophages play an important role.

# References

Abdelaziz, H. M., Gaber, M., Abd-Elwakil, M. M., Mabrouk, M. T., Elgohary, M. M., Kamel, N. M., Kabary, D. M., Freag, M. S., Samaha, M. W., Mortada, S. M., Elkhodairy, K. A., Fang, J., Elzoghby, A. O. (2018). Inhalable particulate drug delivery systems for lung cancer therapy: Nanoparticles, microparticles, nanocomposites and nanoaggregates. *Journal of Controlled Release, 269*, 374-392.

Aberle DR, A. A., Berg CD, Black WC, Clapp JD, Fagerstrom RM, Gareen IF, Gatsonis C, Marcus PM, Sicks JD National Lung Screening Trial Research Team. (2011). Reduced Lung-Cancer Mortality with Low-Dose Computed Tomographic Screening. *New England Journal of Medicine, 365*(5), 395-409.

Andón, F. T., Digifico, E., Maeda, A., Erreni, M., Mantovani, A., Alonso, M. J., & Allavena, P. (2017). Targeting tumor associated macrophages: The new challenge for nanomedicine. *Seminars in Immunology, 34*, 103-113.

Arastéh, K. (2013). *Innere Medizin*. Stuttgart: Thieme.

Argyo, C., Weiss, V., Bräuchle, C., & Bein, T. (2014). Multifunctional Mesoporous Silica Nanoparticles as a Universal Platform for Drug Delivery. *Chemistry of Materials, 26*(1), 435-451.

Auvynet, C., Baudesson de Chanville, C., Hermand, P., Dorgham, K., Piesse, C., Pouchy, C., Carlier, L., Poupel, L., Barthelemy, S., Felouzis, V., Lacombe, C., Sagan, S., Salomon, B., Deterre, P. Sennlaub, F., Combadiere, C. (2016). ECL1i, d(LGTFLKC), a novel, small peptide that specifically inhibits CCL2-dependent migration. *FASEB J, 30*(6), 2370-2381.

Bertrand, N., & Leroux, J.-C. (2012). The journey of a drug-carrier in the body: An anatomo-physiological perspective. *Journal of Controlled Release, 161*(2), 152-163.

Blakely, C. M., Watkins, T. B. K., Wu, W., Gini, B., Chabon, J. J., McCoach, C. E., McGranahan, N., Wilson, G. A., Birkbak, N. J., Olivas, V. R., Rotow, J., Maynard, A., Wang, V., Gubens, M. A., Banks, K. C., Lanman, R. B., Caulin, A. F., John, J. St., Cordero, A. R., Giannikopoulos, P., Simmons, A. D., Mack, P. C., Gandara, D. R., Husain, H., Doebele, R. C., Riess, J. W., Diehn, M., Swanton, C.,d Bivona, T. G. (2017). Evolution and clinical impact of co-occurring genetic alterations in advanced-stage EGFR-mutant lung cancers. *Nature genetics, 49*(12), 1693-1704.

Bolukbas, D. A., & Meiners, S. (2015). Lung cancer nanomedicine: potentials and pitfalls. *Nanomedicine (Lond), 10*(21), 3203-3212.

Cauda, V., Schlossbauer, A., Kecht, J., Zurner, A., & Bein, T. (2009). Multiple core-shell functionalized colloidal mesoporous silica nanoparticles. *J Am Chem Soc, 131*(32), 11361-11370.

Charo, I. F., Myers, S. J., Herman, A., Franci, C., Connolly, A. J., & Coughlin, S. R. (1994). Molecular cloning and functional expression of two monocyte chemoattractant protein 1 receptors reveals alternative splicing of the carboxyl-terminal tails. *Proc Natl Acad Sci U S A, 91*(7), 2752-2756.

Chen, Z., Fillmore, C. M., Hammerman, P. S., Kim, C. F., & Wong, K. K. (2014). Non-small-cell lung cancers: a heterogeneous set of diseases. *Nat Rev Cancer, 14*(8), 535-546.

Cheng, C. J., Tietjen, G. T., Saucier-Sawyer, J. K., & Saltzman, W. M. (2015). A holistic approach to targeting disease with polymeric nanoparticles. *Nat Rev Drug Discov, 14*(4), 239-247.

Chung, K. F., Seiffert, J., Chen, S., Theodorou, I. G., Goode, A. E., Leo, B. F., McGilvery, C. M., Hussain, F., Wiegman, C., Rossios, C., Zhu, J., Gong, J., Tariq, F., Yufit, V., Monteith, A. J., Hashimoto, T., Skepper, J. N., Ryan, M. P., Zhang, J., Tetley, Teresa D., Porter, A. E. (2017). Inactivation, Clearance, and Functional Effects of Lung-Instilled Short and Long Silver Nanowires in Rats. *ACS Nano, 11*(3), 2652-2664.

Collins, L. G., Haines, C., Perkel, R., & Enck, R. E. (2007). Lung cancer: diagnosis and management. *Am Fam Physician, 75*(1), 56-63.

Conway, E. M., Pikor, L. A., Kung, S. H., Hamilton, M. J., Lam, S., Lam, W. L., & Bennewith, K. L. (2016). Macrophages, Inflammation, and Lung Cancer. *Am J Respir Crit Care Med, 193*(2), 116-130.

Cortez-Retamozo, V., Etzrodt, M., Newton, A., Rauch, P. J., Chudnovskiy, A., Berger, C., Ryan, R. J. H., Iwamoto, Y., Marinelli, B., Gorbatov, R., Forghani, R., Novobrantseva, T. I., Koteliansky, V., Figueiredo, JL., Chen, J. W., Anderson, D. G., Nahrendorf, M. Swirski, Filip K., Weissleder, R., Pittet, M. J. Origins of tumor-associated macrophages and neutrophils. (1091-6490 (Electronic)).

Deshmane, S. L., Kremlev, S., Amini, S., & Sawaya, B. E. (2009). Monocyte chemoattractant protein-1 (MCP-1): an overview. *J Interferon Cytokine Res, 29*(6), 313-326.

Ferlay J, S. I., Ervik M, Dikshit R, Eser S, Mathers C, Rebelo M, Parkin DM, Forman D, Bray F. (2012). Fact Sheet: Estimated Incidence, Mortality and Prevalence Worldwide in 2012. *Fact sheet on Cancer.* Retrieved from http://globocan.iarc.fr/Pages/fact_sheets_cancer.aspx

Forbes, B., O'Lone, R., Allen, P. P., Cahn, A., Clarke, C., Collinge, M., Dailey, L. A., Donnelly, L. E., Dybowski, J., Hassall, D., Hildebrand, D., Jones, R., Kilgour, J., Klapwijk, J., Maier, C. C., McGovern, T., Nikula, K., Parry, J. D., Reed, M. D., Robinson, I., Tomlinson, L., Wolfreys, A. (2014). Challenges for inhaled drug discovery and development: Induced alveolar macrophage responses. *Adv Drug Deliv Rev, 71*, 15-33.

Fridlender, Z. G., Kapoor, V., Buchlis, G., Cheng, G., Sun, J., Wang, L. C., Singhal, S., Snyder, L. A., Albelda, S. M. (2011). Monocyte chemoattractant protein-1 blockade inhibits lung cancer tumor growth by altering macrophage phenotype and activating CD8+ cells. *Am J Respir Cell Mol Biol, 44*(2), 230-237.

Garassino, M. C., Cho, B., Kim, J.H., Mazières, J., Vansteenkiste, J., Lena, H., Corral, J. J., Gray, J. E., Powderly, J., Chouaid, C., Bidoli, P., Wheatley-Price, P., Park, K., Soo, R. A., Huang, Y., Wadsworth, C., Dennis, P.A., Rizvi, N.A., ATLANTIC Investigators. (2018). Durvalumab as third-line or later treatment for advanced non-small-cell lung cancer (ATLANTIC): an open-label, single-arm, phase 2 study. *The Lancet Oncology, 19*(4), 521-536.

Garon, E. B., Rizvi, N. A., Hui, R., Leighl, N., Balmanoukian, A. S., Eder, J. P., Patnaik, A., Aggarwal, C., Gubens, M., Horn, L., Carcereny, E., Ahn, M., Felip, E., Lee, J., Hellmann, M. D., Hamid, O., Goldman, J. W., Soria, J., Dolled-Filhart, M., Rutledge, R. Z., Zhang, J., Lunceford, J. K., Rangwala, R., Lubiniecki, G. M., Roach, C., Emancipator, K., Gandhi, L. (2015). Pembrolizumab for the Treatment of Non–Small-Cell Lung Cancer. *New England Journal of Medicine, 372*(21), 2018-2028.

Giard, D. J., Aaronson, S. A., Todaro, G. J., Arnstein, P., Kersey, J. H., Dosik, H., & Parks, W. P. (1973). In Vitro Cultivation of Human Tumors: Establishment of Cell Lines Derived From a Series of Solid Tumors2. *JNCI: Journal of the National Cancer Institute, 51*(5), 1417-1423.

Gottstein, C., Wu, G., Wong, B. J., & Zasadzinski, J. A. (2013). Precise Quantification of Nanoparticle Internalization. *ACS Nano, 7*(6), 4933-4945.

Grivennikov, S. I., Greten, F. R., & Karin, M. (2010). Immunity, inflammation, and cancer. *Cell, 140*(6), 883-899.

Hanahan, D., & Coussens, L. M. (2012). Accessories to the crime: functions of cells recruited to the tumor microenvironment. *Cancer Cell, 21*(3), 309-322.

Hanahan, D., & Weinberg, R. A. (2000). The hallmarks of cancer. *Cell, 100*(1), 57-70.

Hanahan, D., & Weinberg, R. A. (2011). Hallmarks of cancer: the next generation. *Cell, 144*(5), 646-674.

Heldin, C.-H., Rubin, K., Pietras, K., & Östman, A. (2004). High interstitial fluid pressure — an obstacle in cancer therapy. *Nature Reviews Cancer, 4*, 806.

Herold, G. (2017). *Innere Medizin*. Köln: Herold, Gerd.

Hiratsuka, S., Ishibashi, S., Tomita, T., Watanabe, A., Akashi-Takamura, S., Murakami, M., Kijima, H., Miyake, K., Aburatani, H., Maru, Y. (2013). Primary tumours modulate innate immune signalling to create pre-metastatic vascular hyperpermeability foci. *Nat Commun, 4*, 1853.

Hirsch, F. R., Scagliotti, G. V., Mulshine, J. L., Kwon, R., Curran, W. J., Wu, Y.-L., & Paz-Ares, L. (2016). Lung cancer: current therapies and new targeted treatments. *The Lancet*.

Hirsch, F. R., Suda, K., Wiens, J., & Bunn, P. A. (2016). New and emerging targeted treatments in advanced non-small-cell lung cancer. *The Lancet, 388*(10048), 1012-1024.

Jain, R. K., & Stylianopoulos, T. (2010). Delivering nanomedicine to solid tumors. *Nature reviews. Clinical oncology, 7*(11), 653-664.

Johnson, L., Mercer, K., Greenbaum, D., Bronson, R. T., Crowley, D., Tuveson, D. A., & Jacks, T. (2001). Somatic activation of the K-ras oncogene causes early onset lung cancer in mice. *Nature, 410*(6832), 1111-1116.

Kuzmov, A., & Minko, T. (2015). Nanotechnology approaches for inhalation treatment of lung diseases. *J Control Release, 219*, 500-518.

Lammers, T., Kiessling, F., Hennink, W. E., & Storm, G. (2012). Drug targeting to tumors: principles, pitfalls and (pre-) clinical progress. *J Control Release, 161*(2), 175-187.

Landesman-Milo, D., Ramishetti, S., & Peer, D. (2015). Nanomedicine as an emerging platform for metastatic lung cancer therapy. *Cancer Metastasis Rev, 34*(2), 291-301.

Langer, C. J. (2015). Emerging Immunotherapies in the Treatment of Non–small Cell Lung Cancer (NSCLC): The Role of Immune Checkpoint Inhibitors. *American Journal of Clinical Oncology, 38*(4).

Leitlinienprogramm Onkologie, 2017. from Deutsche Krebsgesellschaft, Deutsche Krebshilfe, AWMF http://leitlinienprogramm-onkologie.de/Lungenkarzinom.98.0.html

Leuschner, F., Dutta, P., Gorbatov, R., Novobrantseva, T. I., Donahoe, J. S., Courties, G., Lee, K. M., Kim, J. I., Markmann, J. F., Marinelli, B., Panizzi, P., Lee, W. W., Iwamoto, Y., Milstein, S., Epstein-Barash, H., Cantley, W., Wong, J., Cortez-Retamozo, V., Newton, A., Love, K., Libby, P., Pittet, M. J., Swirski, F. K., Koteliansky, V., Langer, R., Weissleder, R., Anderson, D. G, Nahrendorf, M. (2011). Therapeutic siRNA silencing in inflammatory monocytes in mice. *Nat Biotechnol, 29*(11), 1005-1010.

Mangal, S., Gao, W., Li, T., & Zhou, Q. (2017). Pulmonary delivery of nanoparticle chemotherapy for the treatment of lung cancers: challenges and opportunities. *Acta Pharmacologica Sinica, 38*(6), 782-797.

Marazioti, A., & Stathopoulos, G. T. (2014). Monoclonal antibody targeting of mononuclear cell chemokines driving malignant pleural effusion. *Oncoimmunology, 3*, e29195.

Matsumura, Y., & Maeda, H. (1986). A New Concept for Macromolecular Therapeutics in Cancer Chemotherapy: Mechanism of Tumoritropic Accumulation of Proteins and the Antitumor Agent Smancs. *Cancer research, 46*(12 Part 1), 6387.

Mbawuike, I. N., & Herscowitz, H. B. (1989). MH-S, a murine alveolar macrophage cell line: morphological, cytochemical, and functional characteristics. *J Leukoc Biol, 46*(2), 119-127.

Meindl, C., Öhlinger, K., Ober, J., Roblegg, E., & Fröhlich, E. (2017). Comparison of fluorescence-based methods to determine nanoparticle uptake by phagocytes and non-phagocytic cells in vitro. *Toxicology, 378*, 25-36.

Mitchem, J. B., Brennan, D. J., Knolhoff, B. L., Belt, B. A., Zhu, Y., Sanford, D. E., Belaygorod, L., Carpenter, D. Collins, L., Piwnica-Worms, D., Hewitt, S., Udupi, G. M., Gallagher, W. M., Wegner, C., West, B. L., Wang-Gillam, A., Goedegebuure, S. P., Linehan, David C., DeNardo, D. G. (2013). Targeting tumor-infiltrating macrophages decreases tumor-initiating cells, relieves immunosuppression and improves chemotherapeutic responses. *Cancer research, 73*(3), 1128-1141.

Nichols, J. W., Sakurai, Y., Harashima, H., & Bae, Y. H. (2017). Nano-sized drug carriers: Extravasation, intratumoral distribution, and their modeling. *Journal of Controlled Release, 267*, 31-46.

Noy, R., & Pollard, J. W. (2014). Tumor-associated macrophages: from mechanisms to therapy. *Immunity, 41*(1), 49-61.

Osmani, L., Askin, F., Gabrielson, E., & Li, Q. K. (2017). Current WHO guidelines and the critical role of immunohistochemical markers in the subclassification of non-small cell lung carcinoma (NSCLC): Moving from targeted therapy to immunotherapy. *Seminars in Cancer Biology*.

Ostuni, R., Kratochvill, F., Murray, P. J., & Natoli, G. (2015). Macrophages and cancer: from mechanisms to therapeutic implications. *Trends Immunol, 36*(4), 229-239.

Pardoll, D. M. (2012). The blockade of immune checkpoints in cancer immunotherapy. *Nature reviews. Cancer, 12*(4), 252-264.

Pickup, M. W., Mouw, J. K., & Weaver, V. M. (2014). The extracellular matrix modulates the hallmarks of cancer. *EMBO Reports, 15*(12), 1243-1253.

Popović, Z., Liu, W., Chauhan, V. P., Lee, J., Wong, C., Greytak, A. B., Insin, N., Nocera, D. G., Fukumura, D., Jain, R. K., Bawendi, M. G. (2010). A nanoparticle size series for in vivo fluorescence imaging. *Angewandte Chemie (International ed. in English), 49*(46), 8649-8652.

Qian, B. Z., Li, J., Zhang, H., Kitamura, T., Zhang, J., Campion, L. R., Kaiser, E. A., Snyder, L. A., Pollard, J. W. (2011). CCL2 recruits inflammatory monocytes to facilitate breast-tumour metastasis. *Nature, 475*(7355), 222-225.

Qian, B. Z., & Pollard, J. W. (2010). Macrophage diversity enhances tumor progression and metastasis. *Cell, 141*(1), 39-51.

Quail, D. F., & Joyce, J. A. (2013). Microenvironmental regulation of tumor progression and metastasis. *Nat Med, 19*(11), 1423-1437.

Remark, R., Becker, C., Gomez, J. E., Damotte, D., Dieu-Nosjean, M. C., Sautes-Fridman, C., Fridman, W. H., Powell, C. A., Altorki, N. K., Merad, M., Gnjatic, S. (2015). The non-small cell lung cancer immune contexture. A major determinant of tumor characteristics and patient outcome. *Am J Respir Crit Care Med, 191*(4), 377-390.

Roblek, M., Strutzmann, E., Zankl, C., Adage, T., Heikenwalder, M., Atlic, A., Weis, R., Kungl, A., Borsig, L. (2016). Targeting of CCL2-CCR2-Glycosaminoglycan Axis Using a CCL2 Decoy Protein Attenuates Metastasis through Inhibition of Tumor Cell Seeding. *Neoplasia, 18*(1), 49-59.

Salvati, A., Pitek, A. S., Monopoli, M. P., Prapainop, K., Bombelli, F. B., Hristov, D. R., Kelly, P. M., Åberg, C., Mahon, E., Dawson, K. A. (2013). Transferrin-functionalized nanoparticles lose their targeting capabilities when a biomolecule corona adsorbs on the surface. *Nature Nanotechnology, 8*, 137.

Schlossbauer, A., Kecht, J., & Bein, T. (2009). Biotin-avidin as a protease-responsive cap system for controlled guest release from colloidal mesoporous silica. *Angew Chem Int Ed Engl, 48*(17), 3092-3095.

Schmall, A., Al-Tamari, H. M., Herold, S., Kampschulte, M., Weigert, A., Wietelmann, A., Vipotnik, N., Grimminger, F., Seeger, W., Pullamsetti, S. S., Savai, R. (2015). Macrophage and cancer cell cross-talk via CCR2 and CX3CR1 is a fundamental mechanism driving lung cancer. *Am J Respir Crit Care Med, 191*(4), 437-447.

Siegel, R. L., Miller, K. D., & Jemal, A. (2017). Cancer Statistics, 2017. *CA Cancer J Clin, 67*(1), 7-30.

Spira, A., Halmos, B., & Powell, C. A. (2015). Update in Lung Cancer 2014. *American Journal of Respiratory and Critical Care Medicine, 192*(3), 283-294.

Spira, A., Halmos, B., & Powell, C. A. (2016). Update in Lung Cancer 2015. *Am J Respir Crit Care Med, 194*(6), 661-671.

Tenzer, S., Docter, D., Kuharev, J., Musyanovych, A., Fetz, V., Hecht, R., Schlenk, F., Fischer, D., Kiouptsi, K., Reinhardt, C., Landfester, K., Schild, H., Maskos, M., Knauer, Shirley K., Stauber, R. H. (2013). Rapid formation of plasma protein corona critically affects nanoparticle pathophysiology. *Nature Nanotechnology, 8*, 772.

The Cancer Genome Atlas Research, N. (2014). Comprehensive molecular profiling of lung adenocarcinoma. *Nature, 511*, 543.

Torchilin, V. P. (2014). Multifunctional, stimuli-sensitive nanoparticulate systems for drug delivery. *Nat Rev Drug Discov, 13*(11), 813-827.

Travis William D., B. E., Müller-Hermelink H. Konrad, Curtis C. Harris. (2015). World Health Organization Classification of Tumours. Pathology and Genetics of Tumours of the Lung, Pleura, Thymus and Heart *World Health Organization Classification of Tumours*.

Uhl, F. E., Vierkotten, S., Wagner, D. E., Burgstaller, G., Costa, R., Koch, I., Lindner, M., Meiners, S., Eickelberg, O., Konigshoff, M. (2015). Preclinical validation and imaging of Wnt-induced repair in human 3D lung tissue cultures. *Eur Respir J, 46*(4), 1150-1166.

van Rijt, S. H., Bölükbas, D. A., Argyo, C., Datz, S., Lindner, M., Eickelberg, O., Königshoff, M., Bein, T., Meiners, S. (2015). Protease-Mediated Release of Chemotherapeutics from Mesoporous Silica Nanoparticles to ex Vivo Human and Mouse Lung Tumors. *ACS Nano, 9*(3), 2377-2389.

van Rijt, S. H., Bolukbas, D. A., Argyo, C., Wipplinger, K., Naureen, M., Datz, S., Eickelberg, O., Meiners, S., Bein, T., Schmid, O., Stoeger, T. (2016). Applicability of avidin protein coated mesoporous silica nanoparticles as drug carriers in the lung. *Nanoscale, 8*(15), 8058-8069.

Walkey, C. D., Olsen, J. B., Song, F., Liu, R., Guo, H., Olsen, D. W. H., Cohen, Y., Emili, A., Chan, W. C. W. (2014). Protein Corona Fingerprinting Predicts the Cellular Interaction of Gold and Silver Nanoparticles. *ACS Nano, 8*(3), 2439-2455.

Welsch, U., & Deller, T. (2014). *Lehrbuch Histologie : mit 49 Tabellen* (4. Aufl. ed.). München: Elsevier, Urban & Fischer.

Wicki, A., Witzigmann, D., Balasubramanian, V., & Huwyler, J. (2015). Nanomedicine in cancer therapy: challenges, opportunities, and clinical applications. *J Control Release, 200*, 138-157.

Wilhelm, S., Tavares, A. J., Dai, Q., Ohta, S., Audet, J., Dvorak, H. F., & Chan, W. C. W. (2016). Analysis of nanoparticle delivery to tumours. *Nature Reviews Materials, 1*, 16014.

Wolf, M. J., Hoos, A., Bauer, J., Boettcher, S., Knust, M., Weber, A., Simonavicius, N., Schneider, C., Lang, M., Stürzl, M., Croner, R. S., Konrad, A., Manz, M.G., Moch, H., Aguzzi, A., van Loo, G., Pasparakis, M., Prinz, M., Borsig, L. Heikenwalder, M. (2012). Endothelial CCR2 signaling induced by colon carcinoma cells enables extravasation via the JAK2-Stat5 and p38MAPK pathway. *Cancer Cell, 22*(1), 91-105.

Woods, A., Patel, A., Spina, D., Riffo-Vasquez, Y., Babin-Morgan, A., de Rosales, R. T. M., Sunassee, K., Clark, S., Collins, H., Bruce, K., Dailey, L. A., Forbes, B. (2015). In vivo biocompatibility, clearance, and biodistribution of albumin vehicles for pulmonary drug delivery. *Journal of Controlled Release, 210*, 1-9.

Yang, Y., & Yu, C. (2016). Advances in silica based nanoparticles for targeted cancer therapy. *Nanomedicine, 12*(2), 317-332.

Yu, M., & Zheng, J. (2015). Clearance Pathways and Tumor Targeting of Imaging Nanoparticles. *ACS Nano, 9*(7), 6655-6674.

Zarogoulidis, P., Chatzaki, E., Porpodis, K., Domvri, K., Hohenforst-Schmidt, W., Goldberg, E. P., Karamanos, N., Zarogoulidis, K. (2012). Inhaled chemotherapy in lung cancer: future concept of nanomedicine. *Int J Nanomedicine, 7*, 1551-1572.

Zhang, Y. N., Poon, W., Tavares, A. J., McGilvray, I. D., & Chan, W. C. (2016). Nanoparticle-liver interactions: Cellular uptake and hepatobiliary elimination. *J Control Release, 240*, 332-348.

# Abbreviations

| | |
|---|---|
| 3D-LTC | 3D lung tissue cultures |
| ADC | Adenocellcarcinoma |
| AVI | Avidin coated mesoporous silica nanoparticles |
| BCA | Bicinchoninic acid assay |
| BRAF | V-Raf murine sarcoma viral oncogene homolog B |
| CCL18 | C-C motif chemokine ligand 18 |
| CCL2 | C-C motif chemokine ligand 2 |
| CCL9 | C-C motif chemokine ligand 9 |
| CCR2 | C-C chemokine receptor type 2 |
| CD68 | Cluster of differentiation 68 |
| CDK6 | Cell division protein kinase 6 |
| CEA | Carcioembryonic antigen |
| CK5/6 | Cytokeratine 5 and 6 |
| COPD | Chronic obstructive pulmonary disease |
| CSF1 | Colony stimulating factor |
| CT | Computer tomography |
| DAPI | 4′,6-Diamidin-2-phenylindol |
| DDR2 | Discoidin domain-containing receptor 2 |

| | |
|---|---|
| DMEM | Dulbecco's modified eagle medium |
| DMSO | Dimethyl sulfoxide |
| DTT | Dithiothreitol |
| ECL | Electrochemiluminescence |
| ECM | Extra cellular matrix |
| EDTA | Ethylenediaminetetraacetate |
| EGF | Epidermal growth factor |
| EGFR | Epidermal growth factor receptor |
| EPR | Enhanced permeability and retention |
| FBS | Fetal bovine serum |
| FCS | Fetal calf serum |
| FGF | Fibroblast growth factor |
| FGFR1 | Fibroblast growth factor receptor 1 |
| FGFR2 | Fibroblast growth factor receptor 2 |
| FGFR3 | Fibroblast growth factor receptor 3 |
| GM-CSF | Granulocyte-macrophage colony stimulating factor |
| H&E | Hematoxylin and Eosin |
| HER2 | Receptor tyrosine-protein kinase erbB-2 |
| HRCT | High resolution computer tomography |

| | |
|---|---|
| HRP | Horseradish peroxidase |
| IF | Immunofluorescence |
| IHC | Immunohistochemistry |
| IgG | Immunoglobulin G |
| IL10 | Interleukine 10 |
| IL3 | Interleukine 3 |
| IL4 | Interleukine 4 |
| K-ras | Kirsten rat sarcoma viral oncogene homolog |
| LHRHR | luteinizing hormone releasing hormone receptor |
| LKb1 | Liver kinase b 1 |
| MMPs | Matrix metalloproteinases |
| MRI | Magnetic resonance imaging |
| MSNs | Mesoporous silica nanoparticles |
| NSCLC | Non-small cell lung cancer |
| p53 | Tumor suppressor p53 |
| PBS | Phosphate buffer solution |
| PD-1 | Programmed cell death protein 1 |
| PDL-1 | Programmed cell death ligand 1 |
| PEG | Polyethylene glycol |

| | |
|---|---|
| PET | Positron emission tomography |
| PIK3 | Phosphatidylinositol 3-kinase |
| PIK3CA | Phosphatidylinositol 3-kinase catalytic subunit |
| RIPA | Radioimmunoprecipitation assay |
| RPM | Revolutions per minute |
| RPMI | Roswell Park Memorial Institute medium |
| SCC | Squamous cell carcinoma |
| SCLC | Small cell lung cancer |
| SDS | Sodiumdodecylsulfate |
| SEM | Standard error of the mean |
| SHS | second hand smoke |
| TAMs | Tumor-associated macrophages |
| TBS | Tris-buffered saline |
| TGF-beta | transforming growth factor beta |
| TP53 | Tumor protein 53 |
| TTF1 | Thyroid transcription factor 1 |
| VEGF | Vascular endothelial growth factor |
| WB | Western blot |
| WT | Wild type |

# Acknowledgments

First of all, I would like to thank my supervisors Silke Meiners and Deniz Bölükbas for their support, advice and instructions throughout the last years. This thesis could have not been written without their constant help and I am mostly grateful for what I have learned from them.

In addition, I would like to thank Oliver Eickelberg and Antje Brand for giving me the chance to write my thesis at the Comprehensive Pneumology Center and for their supervision throughout this process. I am further thankful for the help and inspiration of the CPC research school team Camille Beunèche, and Doreen Franke.

In addition, I would like to address my thanks to our collaborators from the Bein Lab at the Physical Chemistry Department at the LMU. I would specially like to thank Stefan Datz for producing the used MSNs and kindly providing data.

My appreciation extends to my lab mates Alessandra Mossina, Amal Houssaini Christina Lukas, Ilona Kammerl, Korbinian Berschneider, Thomas Meul, and Vanessa Welk, who provided me with important knowledge and feedback and who made my time at the CPC greatly memorable.

Last but not least, I would like to thank my family and my friends, who supported me through the last years, who proofread this work and who always believed in me.

# Eidesstattliche Erklärung

Hiermit erkläre ich, Charlotte Meyer-Schwickerath, an Eides statt, dass ich die vorliegende Dissertation mit dem Thema

„Validation of CCR2-targeted Mesoporous Silica Nanoparticles

for Lung Cancer Therapy“

selbstständig verfasst, mich außer der angegebenen keiner weiteren Hilfsmittel bedient und alle Erkenntnisse, die aus dem Schrifttum ganz oder annähernd übernommen sind, als solche kenntlich gemacht und nach ihrer Herkunft unter Bezeichnung der Fundstelle einzeln nachgewiesen habe.

Ich erkläre des Weiteren, dass die hier vorgelegte Dissertation nicht in gleicher oder in ähnlicher Form bei einer anderen Stelle zur Erlangung eines akademischen Grades eingereicht wurde.

Köln, 13.11.2019 Charlotte Meyer-Schwickerath

Ort/Datum Unterschrift